

## GAMMA-RAY BURSTS FROM HIGH-VELOCITY NEUTRON STARS

T. BULIK<sup>1</sup> AND D. Q. LAMB

Department of Astronomy and Astrophysics, University of Chicago, 5640 South Ellis Avenue, Chicago, IL 60637; Tomek\_Bulik@camk.edu.pl,  
lamb@oddjob.uchicago.edu

AND

P. S. COPPI

Department of Astronomy, Yale University, P.O. Box 208101, New Haven, CT 06520; coppi@blazar.astro.yale.edu

Received 1997 July 7; accepted 1998 April 30

### ABSTRACT

We investigate the viability of Galactic corona models of gamma-ray bursts by calculating the spatial distribution expected for a population of high-velocity neutron stars born in the Galactic disk and moving in a gravitational potential that includes contributions from the bulge, disk, and dark matter halo of our Galaxy and also from these same components of our neighboring galaxy M31. We consider two classes of models: one in which the bursts radiate isotropically and one in which the bursts are beamed. We place constraints on these models by comparing the expected brightness and angular distributions with the data in the BATSE 3B catalog. We find that if the bursts radiate isotropically, then the Galactic corona model can reproduce the BATSE peak flux and angular distributions for neutron star kick velocities  $v_{\text{kick}} \gtrsim 800 \text{ km s}^{-1}$ , source turn-on ages  $t_{\text{on}} \gtrsim 20 \text{ Myr}$ , and BATSE sampling distances  $130 \text{ kpc} \lesssim d_{\text{max}} \lesssim 350 \text{ kpc}$ . If the bursts are instead beamed with an opening half-angle  $\theta_b$ , no turn-on age is required, and the model can reproduce the BATSE data for  $15^\circ \lesssim \theta_b \lesssim 20^\circ$  and  $80 \text{ kpc} \lesssim d_{\text{max}} \lesssim 250 \text{ kpc}$ .

*Subject headings:* Galaxy: halo — Galaxy: kinematics and dynamics — gamma rays: bursts — stars: neutron

### 1. INTRODUCTION

Before the launch of the *Compton Gamma-Ray Observatory* (*CGRO*), the prevailing view on the origin of gamma-ray bursts (GRBs) was that the bursts were produced by magnetic neutron stars residing in a thick disk (with scale height  $\approx 2 \text{ kpc}$ ) in the Milky Way (see, e.g., Higdon & Lingefelter 1990; Harding 1991). Upper limits on the rate of faint bursts (Fishman 1979) had already implied that the cumulative brightness distribution of GRBs must roll over at the faint end. Thus it was expected that the BATSE instrument on *CGRO* would see past the edge of the disk distribution and find that the sky distribution of faint GRBs was concentrated in the Galactic plane, confirming the idea that GRBs were Galactic in origin. Instead, the data gathered by BATSE confirmed the existence of a rollover in the cumulative brightness distribution of GRBs but showed that even faint GRBs are distributed isotropically on the sky (Meegan et al. 1992). These results are inconsistent with a thick Galactic disk source population. Consequently, the primary impact of the BATSE results has been to intensify debate about whether GRBs are Galactic or cosmological in origin.

During the past year, the *BeppoSAX* and *Rossi X-Ray Timing Explorer* (*RXTE*) satellites have rapidly disseminated small positional error circles for nine GRBs, and fading X-ray and optical sources have been discovered in some of them. Many of the bursts appear to have fading X-ray sources associated with them (see, e.g., Frontera et al. 1998), but these X-ray sources have so far provided no information about the distance scale to the bursts. A few of the bursts appear to have fading optical sources associated with them, and while more information has been gleaned

from these sources, the burst distance scale implied by these optical sources is still ambiguous. For example, Groot et al. (1997) and Metzger et al. (1997a) discovered an extended nebulosity coincident with the position of GRB 970228. The nebulosity has been interpreted as the distant host galaxy of the burst source. But reports that the brightness and size of the nebulosity may have decreased following the burst (Metzger et al. 1997b; Sahu et al. 1997; Fruchter et al. 1997) are inconsistent with this interpretation and indeed with a cosmological distance scale for the burst source, if the nebulosity is associated with it.

On the other hand, Metzger et al. (1997c) discovered several absorption lines in the optical spectrum of a fading optical source coincident with the position of GRB 970508. The wavelengths of these lines agree with those expected for absorption due to intervening gas at a redshift  $z = 0.8$ . Clearly this optical transient lies at a redshift  $z = 0.8$  or greater, implying a cosmological distance scale for GRB 970508 if this optical transient is associated with the burst source. However, it is not certain that the optical transient is associated with the burst source. Some active galaxies can behave in this manner. For example, at the time of the GRB, the radio, optical, and X-ray properties of the optical transient resembled those of BL Lacs; these objects are known to be highly variable in the optical and to sometimes fade by factors of 300 or more within several months (D. G. York 1997, private communication). But we know from earlier studies of GRB small error boxes (see, e.g., Schaefer 1992) that many of these do not contain active galaxies and therefore that many GRBs—probably all—do not come from active galaxies. The basic problem is that we know very little about the X-ray and optical behavior of distant, faint, active galaxies. We therefore do not know how often such active galaxies exhibit behavior like that shown by the optical transient in this case and, therefore, the probability that such a spatial and temporal coincidence might happen

<sup>1</sup> Nicolaus Copernicus Astronomical Center, Bartycka 18, 00-716 Warsaw, Poland.

by chance. Future deep optical surveys and continuing rapid optical and radio follow-up observations of small positional error circles provided by *BeppoSAX* and *RXTE* will help to clarify the situation.

Other recent developments tend, in our opinion, to favor the Galactic hypothesis. Earlier observations made with the *Ginga* burst detector provided convincing evidence for the existence of lines in the spectra of a few GRBs (Graziani et al. 1992; Murakami et al. 1988). The automated line search initiated by the BATSE team has now found 12 significant line candidates in the spectra of the 100 brightest bursts seen by the BATSE Spectroscopy Detectors; detailed analyses of several of these candidates indicate that the situation is favorable for the existence of lines in the spectra of GRBs (Briggs et al. 1996; Briggs et al. 1998). The existence of long-lived, stable, harmonically spaced line features in the spectra of some bursts is regarded by many as the strongest evidence that some bursts come from magnetic neutron stars and are therefore Galactic in origin. Also, the results of recent *Hubble Space Telescope* observations of four Interplanetary Network (IPN) burst error boxes (Schaefer et al. 1998) and the results of the deep optical follow-up observations of the *BeppoSAX* and *RXTE* burst positional error circles have made the “no-host” problem (Schaefer 1992; Fenimore et al. 1993) more severe. They strengthen the evidence that GRBs do not come from bright galaxies; the bursts therefore either come from faint galaxies or not from galaxies at all. Then there is the detection by BATSE in late October of 1996 of four events in less than two days, which come from directions that are consistent with a single source. These events can only be interpreted either as evidence for burst repetition (which is impossible in most cosmological models), or for the occurrence of only three bursts, one of which would be longer than any other of the 2000 bursts seen by BATSE (Graziani & Lamb 1998). Finally, there remains the problem of the famous 1979 March 5 event, a soft gamma-ray repeater burst that we know took place locally, but would otherwise be classified as a “classical” GRB (Fenimore, Klebesadel, & Laros 1996).

While the weight of opinion has swung heavily toward a cosmological origin for all GRBs, this swing may be premature. First, as we have discussed above, the observational evidence about whether the bursts are Galactic or cosmological is as yet inconclusive. Second, given the diversity of GRB properties (e.g., durations, intensities, spectra, time histories, and so on), it is possible that the bursts come from several distinct source populations. Indeed, recent detailed analyses of the BATSE data (Loredo & Wasserman 1998a, 1998b) show that it is consistent with two GRB source populations: one Galactic, the other cosmological. (The existence of a highly isotropic, extragalactic burst component significantly weakens the isotropy constraints on any anisotropic Galactic component.) Such a “hybrid” Galactic/cosmological origin for GRBs might resolve the deepening contradictions presented by the observational results described above.

In light of the continuing debate between Galactic and cosmological burst scenarios, the goal of this paper is to examine in detail the most promising Galactic model; namely, the high-velocity neutron star Galactic corona model. Galactic halo models for burst sources were first considered and compared with burst data by Fishman et al. (1978) and Jennings & White (1980). Two origins for bursts

in the Galactic halo have since been considered. The first is a population of relic neutron stars, for example, from Population III stars that were born in the halo during the early stages of the Galaxy’s history (Eichler & Silk 1992; Hartmann, Woosley, & Epstein 1990; Wasserman & Salpeter 1994; Gurevich et al. 1993). The second, on which we focus in this paper, is a population of neutron stars born in the Galactic plane but given a sufficient kick velocity at birth that they escape from the Galaxy (Shklovskii & Mitrofanov 1985).

The latter possibility has received increased attention following the work of Lyne & Lorimer (1994). Using a new model for the electron density in the Milky Way and correcting for the observational bias affecting the determination of radio pulsar velocities, they derived a mean space velocity for young radio pulsars of  $\approx 500 \text{ km s}^{-1}$ , with a significant dispersion about this mean. Based on these results and an analysis of the velocity distribution of pulsars in the neighborhood, Cordes, Chernoff, & Wasserman (1996) conclude that at least 28% of the pulsars in the solar neighborhood will escape from the Galaxy. Support for the existence of a significant number of high-velocity neutrons stars also comes from Frail, Goss, & Whiteoak (1994), who find that many young pulsars are associated with previously unknown supernova remnants. These associations imply a median space velocity for young pulsars of  $\approx 500 \text{ km s}^{-1}$ , with one-third of the sample having velocities greater than  $800 \text{ km s}^{-1}$ . Therefore, regardless of how many relic neutron stars exist in the halo of the Galaxy, today there are likely to be a great many neutron stars that are escaping from the Galaxy and that form a neutron star corona around it.

The main problems facing GRB models based on high-velocity neutron stars born in the Galactic plane are: (1) why only high-velocity neutron stars produce bursts (low-velocity neutron stars are bound to the Galaxy, and they would therefore create a strong Galactic disk anisotropy if they produced bursts), and (2) why young, high-velocity neutron stars produce only a small fraction of the total number of observed bursts (even high-velocity neutron stars born in the Galactic disk remain near it while they are young, and a strong Galactic disk anisotropy would therefore still be detectable if these neutron stars produced a significant fraction of observed bursts). In order to solve the first problem, we must postulate some correlation between the neutron star kick velocity and GRBs; e.g., that a high neutron star kick velocity is only possible when the neutron star has a very large magnetic field, and that a large magnetic field is also essential for producing gamma-ray bursts (Duncan, Li, & Thompson 1993). Proponents of the Galactic corona model have suggested two main ways of solving the second problem: (a) source evolution, in which the neutron star burst rate turns on slowly or not at all until the neutron star is a few tens of millions of years old, so that one sees few bursts from young neutron stars (see, e.g., Li & Dermer 1992; Podsiadlowski, Rees, & Ruderman 1995; Bulik & Lamb 1995, 1996a, 1996b; Coppi, Bulik, & Lamb 1996; Lamb, Bulik, & Coppi 1996); and (b) the beamed emission model, in which bursts are beamed along the direction of the initial neutron star kick velocities, and thus bursts become visible only when the neutron stars are far from the disk (see, e.g., Duncan et al. 1993; Li, Duncan, & Thompson 1994; Li & Duncan 1996a, 1996b; Bulik & Lamb 1996b; Duncan & Li 1997). Podsiadlowski et al.

(1995) have also considered the possibility that the neutron star burst phase lasts a long time ( $\sim$ Gyr, so that bursts from young neutron stars constitute only a small fraction of the total), and that bursts come from a population of weakly bound neutron stars orbiting the Galaxy in extended orbits in a nonspherically symmetric halo potential. Finally, Schaefer (1996) explores the beamed emission model, but argues that the typical kick velocities could be very high,  $\sim 2000 \text{ km s}^{-1}$ ; i.e., that the typical burst distance scale could be  $\sim 1 \text{ Mpc}$ , and the observed burst distribution represents a “Local Group Halo” rather than simply one about our Galaxy.

In this paper we test the viability of such Galactic corona models by calculating the spatial distribution of neutron stars born with high velocities in the Galactic disk and comparing the expected GRB brightness and angular distributions with data from the BATSE 3B catalog. In doing this, we carefully select the data sample that we use so that threshold effects and other systematic effects are minimized. We use a detailed and more realistic model of the gravitational potential of the Galaxy than in previous work. We also include the effects of M31, both as a perturbation to the gravitational potential seen by propagating neutrons stars and as a source of high-velocity neutron stars (some of which may make their way into our Galaxy). Our goal is to carry out a much more extensive exploration of the parameter space than has been done before. In § 2 we discuss the model of the Galaxy that we use, the dynamics of neutron stars in the Galactic halo, the numerical method we use to follow the neutron stars, and the results. In § 3 we present a model parameterization of bursting from high-velocity neutron stars. In § 4 we compare the GRB sky and brightness distributions derived from the BATSE data and those expected in the isotropic and beamed emission models. In § 5 we describe the particular effects that the presence of M31 has on the GRB sky and brightness distributions. In § 6 we discuss our results, and in § 7 we present our conclusions. We have reported several preliminary results of this study in Bulik & Lamb (1995, 1996a, 1996b); Bulik, Coppi, & Lamb (1996); Coppi et al. (1996); and Lamb et al. (1996).

## 2. DYNAMICS OF HIGH-VELOCITY NEUTRON STARS

### 2.1. Neutron Star Birthplaces and Initial Velocities

Since neutron stars are born in supernova explosions, it seems natural to assume that the distribution of neutron star birthplaces traces that of matter in the Galactic disk. Accordingly, we follow Blaes & Madau (1993) and Narayan & Ostriker (1990) and assume that the probability density for a neutron star to be born at cylindrical coordinates  $z$  and  $r$  is a Gaussian in  $z$  and follows the stellar disk density as a function of  $r$ ; i.e.,

$$p(r, z) \propto \exp\left(\frac{-z^2}{2\sigma_z^2}\right) r \exp\left(-\frac{r}{r_d}\right), \quad (1)$$

where  $\sigma_z$  and  $r_d$  are the Gaussian and exponential scale heights of the disk in the vertical and radial directions.

As in previous work, we assume that neutron stars are born with a kick velocity  $v_{\text{kick}}$  (one of the parameters we will explore) that is randomly oriented in the frame locally *corotating* with the disk of our Galaxy. We also assume that M31 acts as an identical source of neutron stars.

### 2.2. Gravitational Potential

The gravitational potential of our Galaxy has been exten-

sively investigated (for a sample review, see Binney & Tremaine 1987). Models of the potential typically include contributions due to the bulge, the disk, and the dark matter halo. Earlier studies of Galactic neutron star propagation (Hartmann et al. 1990; Paczyński 1990; Li et al. 1994; Blaes & Madau 1993; Podsiadlowski et al. 1995) employed the Galactic potential model of Miyamoto & Nagai (1975). In this model, the contributions to the potential from both the disk and the bulge are of the form

$$\Phi = -\frac{GM}{\sqrt{R^2 + [a + (z^2 + b^2)^{1/2}]^2}}, \quad (2)$$

where  $R = (x^2 + y^2)^{1/2}$  is the two-dimensional radius in the disk plane. The potential of the halo component is described by

$$\Phi = \frac{GM_h}{r_h} \left[ \frac{1}{2} \ln\left(1 + \frac{r^2}{r_h^2}\right) + \frac{r_h}{r} \tan^{-1} \frac{r}{r_h} \right]. \quad (3)$$

We find that the Miyamoto & Nagai (1975) potential implies the existence of an extended disk of matter, far beyond the observed Galactic disk. Approximately  $\approx 20\%$  of the mass of this disk lies outside  $r = 20 \text{ kpc}$ , whereas in a more realistic exponential Galactic disk, less than 4% of the mass lies outside 20 kpc. This effect has already been noted (e.g., Binney & Tremaine 1987, p. 44). The density corresponding to the potential of equation (2) falls off as  $r^{-3}$  at large radii, while in more realistic models it falls off exponentially, like the observed light distribution. At large distances, the presence of the extra disk mass results in the gravitational focusing of escaping neutron stars toward the Galactic plane. This effect can be demonstrated by calculating the ratio of the  $z$  component of the gravitational force, obtained using the Miyamoto & Nagai (1975) potential, to that from a point mass for  $r \gg a, b, z$ :

$$\frac{F_z^{\text{MN}}}{F_z^{\text{PM}}} = 1 + \frac{a}{(b^2 + z^2)^{1/2}}, \quad (4)$$

where MN and PM denote Miyamoto & Nagai and point mass potentials, respectively, and  $a$  and  $b$  are parameters describing the Miyamoto & Nagai potential. Typically,  $a \approx 4 \text{ kpc}$  and  $b \approx 0.2 \text{ kpc}$ , so that  $F_z^{\text{MN}}/F_z^{\text{PM}} \rightarrow \approx 20$  as  $z \rightarrow 0$ . The use of the Miyamoto & Nagai (1975) potential distorts the orbits of neutron stars whose initial velocity vectors lie in or near the plane of the disk, and leads to an anisotropic spatial distribution that is entirely an artifact of the unrealistic disk potential (see Fig. 1). Thus, while the Miyamoto & Nagai (1975) potential accurately describes the *local* Galactic environment within  $\sim 10 \text{ kpc}$ , it is not an appropriate potential to use at large distances. For the neutron star corona calculations presented in this paper, we are interested in *both* the local and the long-range details of the potential. Moreover, the accuracy of the isotropy measurements provided by BATSE requires that the model of the Galactic potential be correspondingly accurate.

A more realistic gravitational potential has been presented by Kuijken & Gilmore (1989a); a summary of this model is presented in Table 1. Their model for the halo does not differ significantly from that of Miyamoto & Nagai (1975). However, their model of the disk assumes a simple but realistic form for the density of the disk (namely, that the density decreases exponentially away from the Galactic center and away from the Galactic plane—a doubly expo-

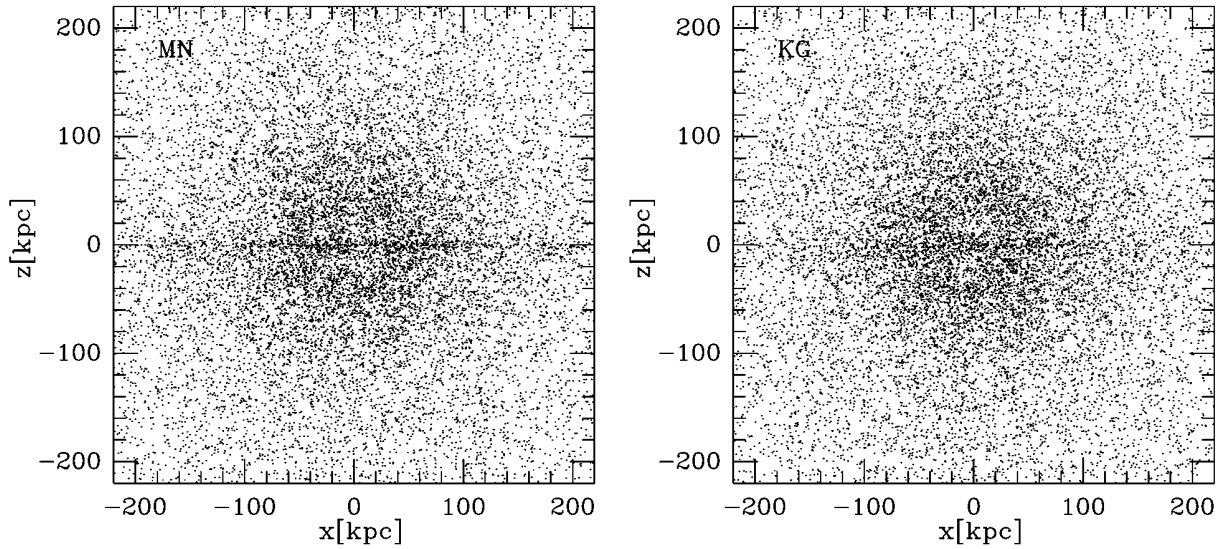


FIG. 1.—Spatial distribution of neutron stars for a kick velocity of  $1000 \text{ km s}^{-1}$  using the Miyamoto & Nagai (1975) model of the Galactic gravitational potential (*left*) and using the Galactic gravitational potential derived from the Kuijken & Gilmore (1989) model of the mass distribution in the Galaxy (*right*). Note the increased concentration of stars in an extended disk due to the focusing described in the text.

nential disk) rather than a simple form for the gravitational potential, as does the model of Miyamoto & Nagai (1975). This leads to some complications when calculating the gravitational potential and force due to such a mass distribution, but the problem can be treated fairly efficiently numerically. This is the potential that we adopt in this paper.

2.3. *Perturbations Due to Neighboring Galaxies*

When considering high-velocity neutron stars that move a large distance from the center of the Galaxy, it is important to consider perturbations to the gravitational potential from neighboring galaxies in the Local Group. At large distances, these perturbations break the axial symmetry of the potential, which has important dynamical implications: it means orbits are neither periodic nor closed (Podsiadlowski et al. 1995). Andromeda (or M31), the other massive galaxy in the Local Group, is probably the dominant perturbation to the potential at large distances. In modeling the gravitational potential, we therefore include the effects of M31 but do not include the effects of small

nearby galaxies like the LMC and SMC. We treat M31 as an identical copy of our Galaxy, located at a distance of 640 kpc in the direction corresponding to Galactic coordinates  $l = 121.17$  and  $b = -21.57$ . The effective gravitational potential of the combined Milky Way-M31 system is then

$$\Phi = \Phi_{\text{MW}}(r) + \Phi_{\text{MW}}(r - r_{\text{M31}}), \quad (5)$$

where  $r$  is the vector distance measured from the center of the Galaxy, and  $r_{\text{M31}}$  is the vector distance of the center of M31 measured from the center of the Galaxy.

2.4. *Numerical Simulations*

In order to study the dynamical motion of neutron stars in the Galactic halo and to compute their resulting spatial distribution, we have developed a computer code that calculates the orbits of a large number of high-velocity neutron stars. The code randomly samples the neutron star birth-place and initial velocity distributions presented above. The number of neutron stars followed in each run is typically 10,000. This number is sufficient to give a statistical accuracy of  $\sim 1\%$  in quantities like the Galactic dipole moment,

TABLE 1  
MODEL OF THE GALAXY USED IN THIS PAPER

Density	Parameters
Disk:	
$\rho = \rho_d \exp\left(-\frac{R}{h_r}\right) \exp\left(-\frac{ z }{z_0}\right)$ .....	$\rho_d = 0.48 M_{\odot} \text{ pc}^{-3}$ $h_r = 4.5 \text{ kpc}$
Bulge (for $Z =  (r/r_s)^2 - 1 $ ):	
$\rho = \rho_s \frac{3.75}{Z^2} \left[ \frac{3-Z}{Z^{1/2}} \left( \ln \frac{1+Z^{1/2}}{(1-Z)^{1/2}} \right) - 3 \right]$ , $r < r_s$ .....	$\rho_s = 193 M_{\odot} \text{ pc}^{-3}$
$\rho = \rho_s$ , $r = r_s$ .....	$r_s = 0.08 \text{ kpc}$
$\rho = \rho_s \frac{3.75}{Z^2} \left\{ \frac{3-Z}{Z^{1/2}} \left[ \tan^{-1} \left( -\frac{1}{Z^{1/2}} \right) + \frac{\pi}{2} \right] - 3 \right\}$ , $r > r_s$ .....	
Halo:	
$\rho = \frac{\rho_c}{1 + (r/r_c)^2}$ , $r < r_{\text{max}}$ .....	$\rho_c = 0.0109 M_{\odot} \text{ pc}^{-3}$
$\rho = 0$ , $r > r_{\text{max}}$ .....	$r_c = 2.019 \text{ kpc}$ $r_{\text{max}} = 100 \text{ kpc}$

although it is not always enough to compute accurately the bright end of the burst brightness distribution (where the number of bursts becomes very small). This should be kept in mind if one uses the exact numerical values given here. To verify that the conclusions we present in this paper are *not* significantly affected by statistical errors, we carried out several runs with up to one million stars. The results are essentially indistinguishable from those presented in this paper.

Using a standard fourth-order Runge-Kutta integration scheme with an adaptive step size, we evolve each star's position using the force computed from our assumed Galactic potential. We checked that our integrator was sufficiently accurate to ensure good energy and angular momentum conservation for many dynamical times. Depending on the temporal resolution we desire, we store the neutron star positions and velocities every 5–10 million years. Since we assume that the gravitational potential is independent of time (although this is not strictly true, since M31 and our Galaxy are falling toward each other), these positions and velocities comprise a template or “Green’s function” that allows us to predict where stars born at a certain time with a particular birthplace and initial velocity will be at a later time. Convolving this template, or Green’s function, with the bursting rate of a neutron star as a function of the time since its birth, we obtain the spatial distribution of observed bursts. The time-consuming task is the calculation of the neutron star orbits, not the convolution of the spatial distribution with the neutron star bursting rate. Therefore, once we have computed and stored a set of templates, we can quickly explore large regions of model parameter space.

### 2.5. Results

We find that the distribution of neutron stars in the Galactic halo depends mainly on three parameters:  $v_{\text{esc}}$ , the escape velocity from the Galaxy;  $v_{\text{rot}}$ , the rotational velocity in the disk; and  $v_{\text{kick}}$ , the neutron star kick velocity at birth. The escape velocity from our Galaxy varies as a function of position in the Galaxy. In the solar neighborhood it is about  $500 \text{ km s}^{-1}$ , and it increases toward the Galactic center. The rotational velocity of the Galactic disk, on the other hand, is roughly constant, with a typical value  $v_{\text{rot}} \sim 220 \text{ km s}^{-1}$ . A neutron star born in the Galactic disk has a net velocity determined not only by the kick it receives in the supernova explosion at its birth, but also by the local disk rotational velocity at which the presupernova star was presumably traveling. The presence of this additional (rotational) velocity component has strong implications for the distribution of neutron stars in the Galactic halo.

In the doubly exponential model of the Galactic disk, the majority of neutron stars are born in a ring at a distance  $\approx 3$  kpc from the Galactic center. Thus, for kick velocities much less than the escape velocity at this radius ( $v_{\text{kick}} \ll 600 \text{ km s}^{-1}$ ), essentially all neutron stars are bound to the Galaxy and form an extended, disklike distribution like that of rotation-powered pulsars. For kick velocities comparable to the escape velocity at this radius ( $v_{\text{kick}} \approx 600 \text{ km s}^{-1}$ ), the situation is more complicated. Depending on the orientation of their kick velocity relative to the local rotational velocity, some neutron stars have a net velocity that exceeds the local  $v_{\text{esc}}$ , and some have a net velocity that is less than it. Thus the distribution of neutron stars consists of a bound fraction that oscillates in the Galactic potential and an unbound fraction that streams out of the Galaxy. When the

kick velocity is much larger than the escape velocity at this radius ( $v_{\text{kick}} \gg 600 \text{ km s}^{-1}$ ), almost all of the neutron stars are unbound and their halo distribution then resembles that of a free ( $\approx$  constant velocity) wind of neutron stars flowing out of the Galaxy. We present examples of the spatial distributions for these three cases in Figure 2. Each panel shows the distribution of an ensemble of  $10^4$  neutron stars  $10^8$  yr after they are born. In the top panel the kick velocity is  $300 \text{ km s}^{-1}$ , in the middle panel it is  $600 \text{ km s}^{-1}$ , and in the bottom panel it is  $1000 \text{ km s}^{-1}$ . The three distributions are very different.

The rotational velocity of the Galactic disk has a very strong influence on the distribution of neutron stars streaming out of the Galaxy. Let us first consider the distribution that neutron stars born at the same time with the same kick velocity  $v_{\text{kick}}$  would have, if the rotational velocity were neglected. As remarked above, most neutron stars are born at a distance  $\approx 3$  kpc from the Galactic center. Since the gravitational potential flattens in the inner region of the Galaxy, the escape velocity for these stars does not depend strongly on their birthplace. To first order, then, the distribution of the stars after a time  $t$  is a “shell” of radius  $r \approx v_{\text{kick}} t$ , with a width comparable to the extent ( $\sim 3$  kpc) of the region in which they were born. Including the rotational velocity of the Galactic disk significantly changes the spatial distribution of the neutron stars in this expanding shell. Depending on the relative orientation of the kick and the rotational velocities, some neutron stars will have initial speeds that are faster than the original kick speed, and some will have initial speeds that are slower. More importantly, the resulting distribution of net (kick plus rotational) velocities is *not* isotropic, because the rotational velocity of the disk affects only the component of the initial velocity that is in the plane of the disk. Consequently, inclusion of the rotational velocity of the disk makes the expanding shell of neutron stars prolate, with an oblate void inside it.

As an illustrative example, we present in Figure 3 the spatial distribution of neutron stars born with a kick velocity  $v_{\text{kick}} = 1200 \text{ km s}^{-1}$  after a time (age) of 50 Myr. The spatial distribution, shown in the top panel, is clearly *non-spherical*; this represents a very important difference between this work and some previous treatments (e.g., Hakkila et al. 1994; Hartmann et al. 1990). The bottom panels in Figure 3 show the contribution to the Galactic dipole and quadrupole moments of the expanding shell of neutron stars as a function of radial distance from the Sun. The three vertical lines in the bottom panels correspond to the radii of the three circles shown in the top panel. Sampling the expanding shell of neutron stars as a function of increasing radial distance from the Sun, one first sees a negative dipole moment (corresponding to an excess of neutron stars in the direction of the Galactic anticenter). The dipole signal decreases with increasing radial distance and vanishes at a radial distance ( $d \sim 60$  kpc) that corresponds to the center of the expanding shell. At still larger radial distances, the dipole moment becomes increasingly positive (corresponding to an excess of neutron stars in the direction of the Galactic center). The quadrupole moment is positive (corresponding to an excess of neutron stars in the directions of the Galactic poles) for radial distances comparable to that of the expanding shell and negative (corresponding to an excess of neutron stars in the direction of the Galactic plane) everywhere else. As a consequence of this complicated behavior, the total (integrated) dipole and

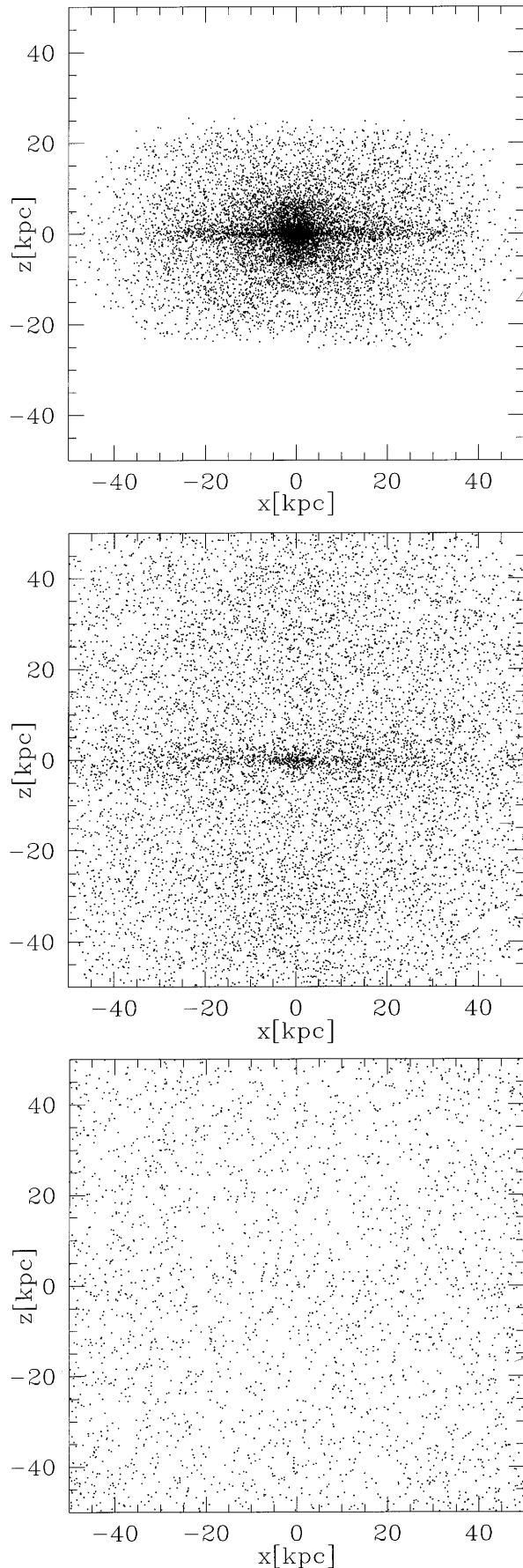


FIG. 2.—Spatial distribution of neutron stars 100 Myr after they are born in the Galactic plane, for kick velocities of  $300 \text{ km s}^{-1}$  (top),  $600 \text{ km s}^{-1}$  (middle), and  $1000 \text{ km s}^{-1}$  (bottom).

quadrupole moments are very close to those expected from an isotropic distribution—even though the Sun is displaced from the center of the Galaxy by  $\approx 8 \text{ kpc}$ . Finally, we note that the expanding shell shown in the top panel of Figure 3 preserves its shape as it expands in time. The main distortion to its shape is due the gravitational pull of M31, which only becomes important when the neutron stars are  $\approx 400 \text{ kpc}$  from us.

### 3. NEUTRON STAR BURST RATE AND BURST LUMINOSITY FUNCTIONS

Given a spatial distribution of neutron stars, the angular distribution and the brightness distribution of GRBs that we actually observe depends on the degree to which the bursts are beamed, the burst rate, and the intrinsic luminosity function of the bursts. Since we know that neutron stars evolve in time (e.g., they cool), it is quite likely that the burst rate and the luminosity function of the bursts evolve in time. Isotropic emission models with a delayed turn-on (see, e.g., Li & Dermer 1992; Podsiadlowski et al. 1995; Bulik & Lamb 1995, 1996a, 1996b; Lamb et al. 1996) and beamed emission models (see, e.g., Duncan et al. 1993; Li et al. 1994; Li & Duncan 1996a, 1996b; Duncan & Li 1997) have been proposed. We consider both possibilities here. We parameterize the burst-active phase in the delayed turn-on model by the bursting turn-on time  $t_{\text{on}}$  and by the bursting turn-off time  $\Delta T$ . We assume a constant bursting rate throughout the burst active phase. The beamed emission model assumes that the burst is beamed parallel and antiparallel to the direction of the neutron star’s kick velocity. In this case, no source evolution is needed: the beaming prevents us from seeing bursts from neutron stars when they are young and near the Galactic plane. The main parameter in the beamed emission model is the opening half-angle  $\theta_b$  of the beamed emission. One can of course explore more complicated isotropic and beamed emission models, but for clarity we consider only the simplest possibilities here. These are sufficient to match the BATSE data.

In principle, the burst luminosity function also plays an important role in determining the observed angular and brightness distributions of the GRBs. Unfortunately, the GRB luminosity function is not well constrained observationally (Loredo & Wasserman 1998a, 1998b). The burst luminosity function is typically modeled as a power law (Hakkila et al. 1995; Loredo & Wasserman 1998a, 1998b),

$$\frac{dN}{dL} = \begin{cases} L^{-\alpha}, & L_{\min} < L < L_{\max}, \\ 0, & \text{elsewhere,} \end{cases} \quad (6)$$

or as a log-normal distribution with a width  $w = L_{\max}/L_{\min}$  (Bulik et al. 1996). The power-law luminosity function behaves like a standard candle when  $\alpha$  is large, whether positive or negative.

In the intermediate case, the luminosity distribution of observed bursts is determined mainly by  $w$ . A log-normal distribution is specified by two parameters: the width  $w$  and the centroid of the distribution.

In order to simplify our analysis, we consider here a simple luminosity function in which the effects of the width of the luminosity function are pronounced: a “top-hat” luminosity function that is constant per decade of luminosity (i.e., that has  $\alpha = -1$ ) over a luminosity range  $w$ . In comparing this model with the data, we characterize the BATSE sampling distance by that for a burst with the geo-

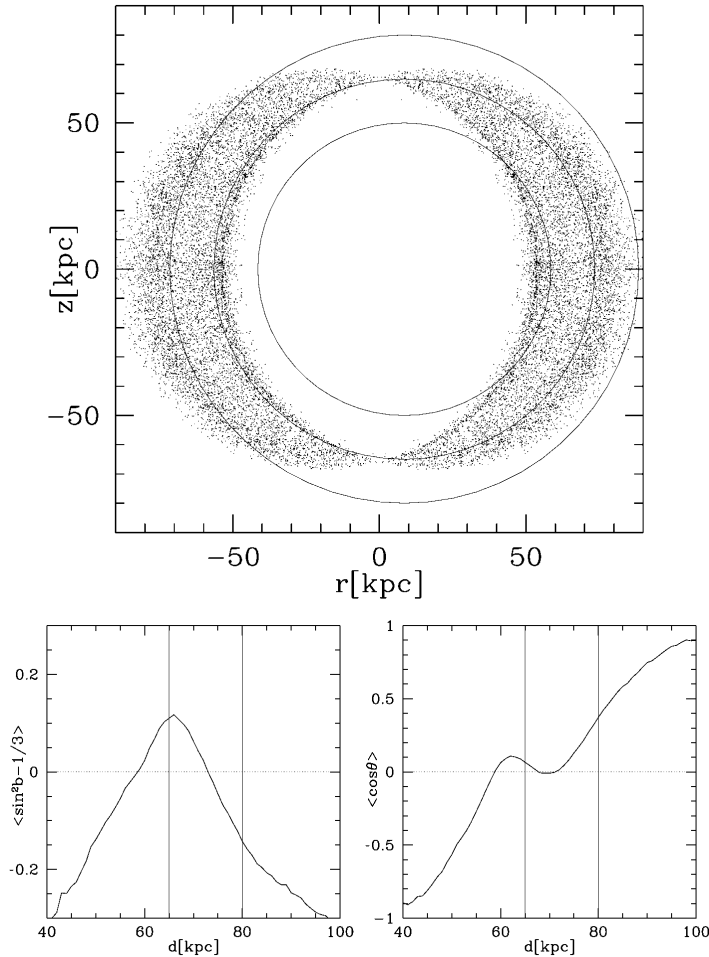


FIG. 3.—*Top panel*: Distribution of neutron stars 50 Myr after they are born in the Galactic disk with a kick velocity of  $1200 \text{ km s}^{-1}$  in the  $(r, z)$  plane, where  $r$  is the radial distance from the axis of the Galaxy in the Galactic plane in the direction of the Sun and  $z$  is the height above the Galactic plane. This distribution corresponds to that formed by taking the three-dimensional distribution of neutron stars and rotating the spatial positions of the neutron stars about the axis of the Galaxy so that all of them lie in the  $(r, z)$  plane. The “shell” of outward moving neutron stars is clearly not spherically symmetric. *Lower panels*: Galactic dipole and quadrupole moments (as measured from the Sun) produced by the three-dimensional distribution of neutron stars for the model parameters shown in the top panel, when one considers only those neutron stars in a shell of radius  $d$  from the Sun. The three vertical lines in the bottom panels correspond to the three (Sun-centered) shells shown in the top panel.

metric average of the minimum and maximum burst luminosities; i.e.,

$$d_{\text{av}} = \left[ \frac{(L_{\text{min}} L_{\text{max}})^{1/2}}{4\pi F_{\text{BATSE}}} \right]^{1/2}, \quad (7)$$

where  $F_{\text{BATSE}}$  is the burst flux at the BATSE detection threshold. We also assume that the burst luminosity does *not* depend on the age of the bursting neutron star. While other luminosity functions are easily imagined, this model is sufficient to provide an insight into the general effects that a spread in burst luminosities has.

#### 4. COMPARISON WITH OBSERVATIONS

##### 4.1. Selection of the Data

We compare our models with a carefully selected data set that is self-consistent (Bulik & Lamb 1995, 1996b; Bulik et al. 1996). Our goal is to minimize threshold and other systematic effects by using a well-defined flux-limited sample. We include only bursts that (1) trigger on the 1024 ms timescale and have  $t_{90} > 1024$  ms; (2) have a measured value of  $F_{\text{pk}}^{1024}$ , the peak flux in 1024 ms, since we adopt it as our brightness measure; and (3) have  $F_{\text{pk}}^{1024} \geq 0.35$  photons

$\text{cm}^{-2} \text{ s}^{-1}$  (Fenimore et al. 1993; in’t Zand & Fenimore 1994). We exclude overwriting bursts, which have a different and high threshold, and MAXBC bursts, which have larger positional errors. We choose the 1024 ms timescale, because BATSE is most sensitive on the longest trigger timescale, and hence the limiting flux is the smallest. The BATSE 3B catalog (Meegan et al. 1996) contains 570 bursts satisfying the above criteria; this set of bursts has Galactic dipole and quadrupole moments  $\langle \cos \theta \rangle = 0.018 \pm 0.0241$  and  $\langle \sin^2 b - \frac{1}{3} \rangle = -0.011 \pm 0.012$ , and a dipole moment toward M31 of  $\langle \cos \theta_{\text{M31}} \rangle = 0.0078 \pm 0.0241$ . The comparisons we show below do not provide estimates of model parameters (i.e., they do not yield best-fit parameter values or parameter confidence regions) but are meant only to be a rough “goodness-of-fit” guide to models that should be tested using a more rigorous approach (e.g., using Bayesian inference methods; see Loredo & Wasserman 1996, 1998a, 1998b).

##### 4.2. Comparison of the Isotropic Emission Model with the BATSE Data

To explore the consistency of the BATSE data with our corona models, we employ a “Green’s function” approach

and consider models with fixed values of the neutron star kick velocity  $v_{\text{kick}}$ , the burst luminosity function width  $w$ , and the bursting turn-off time,  $\Delta T$ . The remaining parameter space for the isotropic emission model is then spanned by the time delay  $t_{\text{on}}$  before bursting begins and the distance  $d_{\text{av}}$  to a typical burst. For each set of the fixed parameters, we therefore present contour plots in the  $(t_{\text{on}}, d_{\text{av}})$  plane, comparing the expected model values and the observed values for (1) the Galactic dipole moment  $\langle \cos \theta \rangle$ , (2) the dipole moment toward M31  $\langle \cos \theta_{\text{M31}} \rangle$ , (3) the Galactic quadrupole moment  $\langle \sin^2 b - \frac{1}{3} \rangle$ , and (4) a Kolmogorov-Smirnoff (KS) consistency test of the model and the observed burst peak flux distribution. In the first three plots, we show contours corresponding to the 1, 2, and 3  $\sigma$  deviations from the observed values, and for the KS test of the peak flux distribution we show contours along which

the model and the data are consistent at the 32%, 5%, and 0.4% probability levels. The consistency of the models with the *Pioneer Venus Orbiter (PVO)* data is addressed in a following section.

We first investigate the behavior of corona models as a function of the neutron star kick velocity. In Figure 4, we present the results for a model in which the neutron stars all have kick velocities of  $600 \text{ km s}^{-1}$ . For such a low kick velocity, a significant fraction of the neutron stars remains bound to the Galaxy (see Fig. 2). This population of neutron stars produces a strong Galactic quadrupole moment, which is inconsistent with the data. The dipole moments can be accommodated by sampling distances that are large enough to see bursts from M31; i.e.,  $d_{\text{max}} \approx 500 \text{ kpc}$ . However, the peak flux distribution fits the data only when  $d_{\text{max}} \approx 25 \text{ kpc}$ , which corresponds to seeing an

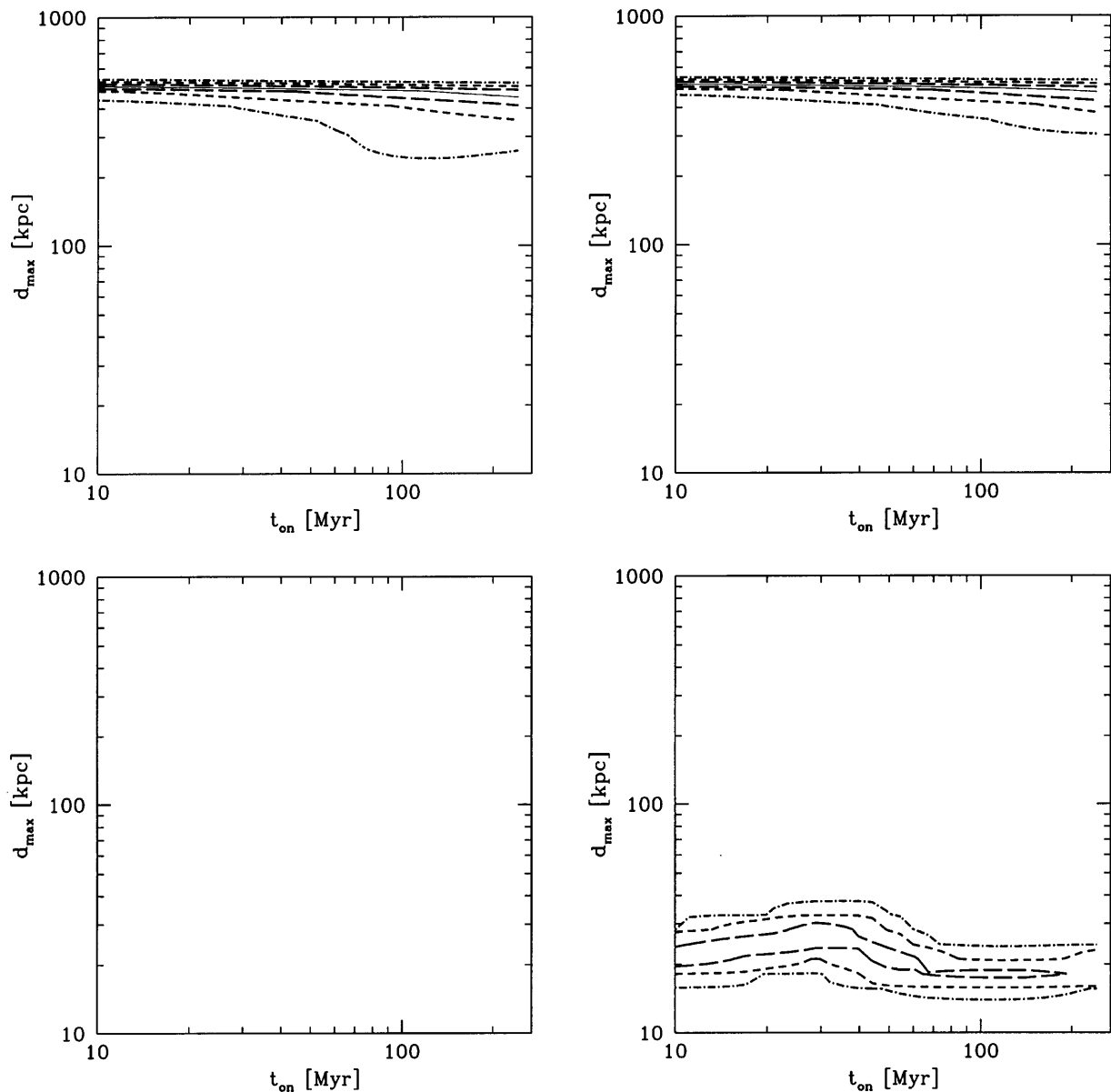


FIG. 4.—Comparison between the Galactic dipole moment (*upper left*), the dipole moment relative to M31 (*upper right*), the Galactic quadrupole moment (*lower left*), and the distribution of burst peak fluxes (*lower right*) derived from the BATSE data and those expected in the isotropic emission model for a kick velocity  $v_{\text{kick}} = 600 \text{ km s}^{-1}$ , a turn-off time  $\Delta T = 500 \text{ Myr}$ , and a luminosity function of zero width, in the  $(t_{\text{on}}, d_{\text{max}})$  plane. The contours in the first three panels delineate the regions within which the model deviates from the BATSE values by less than 1  $\sigma$  (*long-dashed line*), 2  $\sigma$  (*short-dashed line*), and 3  $\sigma$  (*dash-dotted line*); along the thin solid lines, the model has the exact value derived from the BATSE 3B data. The contours in the fourth panel delineate the regions within which the BATSE data and the model are consistent at the 32%, 5%, and 0.4% probability levels.



extended disk of bound stars orbiting the Milky Way. Hence, regardless of the choice of other parameters, there is no way to match the isotropy of the BATSE bursts when the bulk of the neutron stars have velocities  $\lesssim 600 \text{ km s}^{-1}$ .

The parameter space consistent with the BATSE 3B data opens up as the typical neutron star kick velocity increases. We find that corona models become consistent with the data beginning at kick velocities  $\sim 800 \text{ km s}^{-1}$ . By a kick velocity  $\sim 1000 \text{ km s}^{-1}$ , the region of parameter space consistent with the data is quite large. In Figures 5 and 6, we show the results for isotropic emission models with a kick velocity of  $1000 \text{ km s}^{-1}$ , and burst active phases lasting for 500 Myr and 2000 Myr, respectively. There is a large amount of parameter space for which the Galactic quadrupole moment lies within  $1 \sigma$  of the value observed by BATSE. This is due to the anti-Galactic signal that exists in a part of each shell of a given age, as we illustrated in Figure 3. The burst brightness distribution is consistent with that derived from the BATSE 3B data along a diagonal line in the  $(t_{\text{on}}, d_{\text{max}})$  plane. This line arises from the fact that the

burst turn-on time produces a break in the brightness distribution, as the BATSE data requires. Thus the turn-on time determines the typical burst flux (or distance) at the break, and the BATSE sampling distance is determined by the ratio of the typical burst flux at the break to the burst flux at the BATSE threshold. Interestingly, when the burst-active phase extends to very long times (see Fig. 6), the observed brightness distribution restricts the BATSE sampling distance  $d_{\text{max}}$  to modest values. This is because bursts from neutron stars coming from M31 create an excess of bursts at low fluxes in such a model. The upper limit on the sampling distance in both the Galactic dipole and the dipole toward M31 is due to two factors: the burst turn-off age and the presence of M31. Because M31 roughly lies in the direction of the Galactic anticenter, the contour plots for the M31 and the Galactic center dipole moments are similar.

Finally, in Figure 7 we present the results for an isotropic emission model with a kick velocity of  $2000 \text{ km s}^{-1}$  and a burst-active phase lasting for 2000 Myr. The isotropy of the

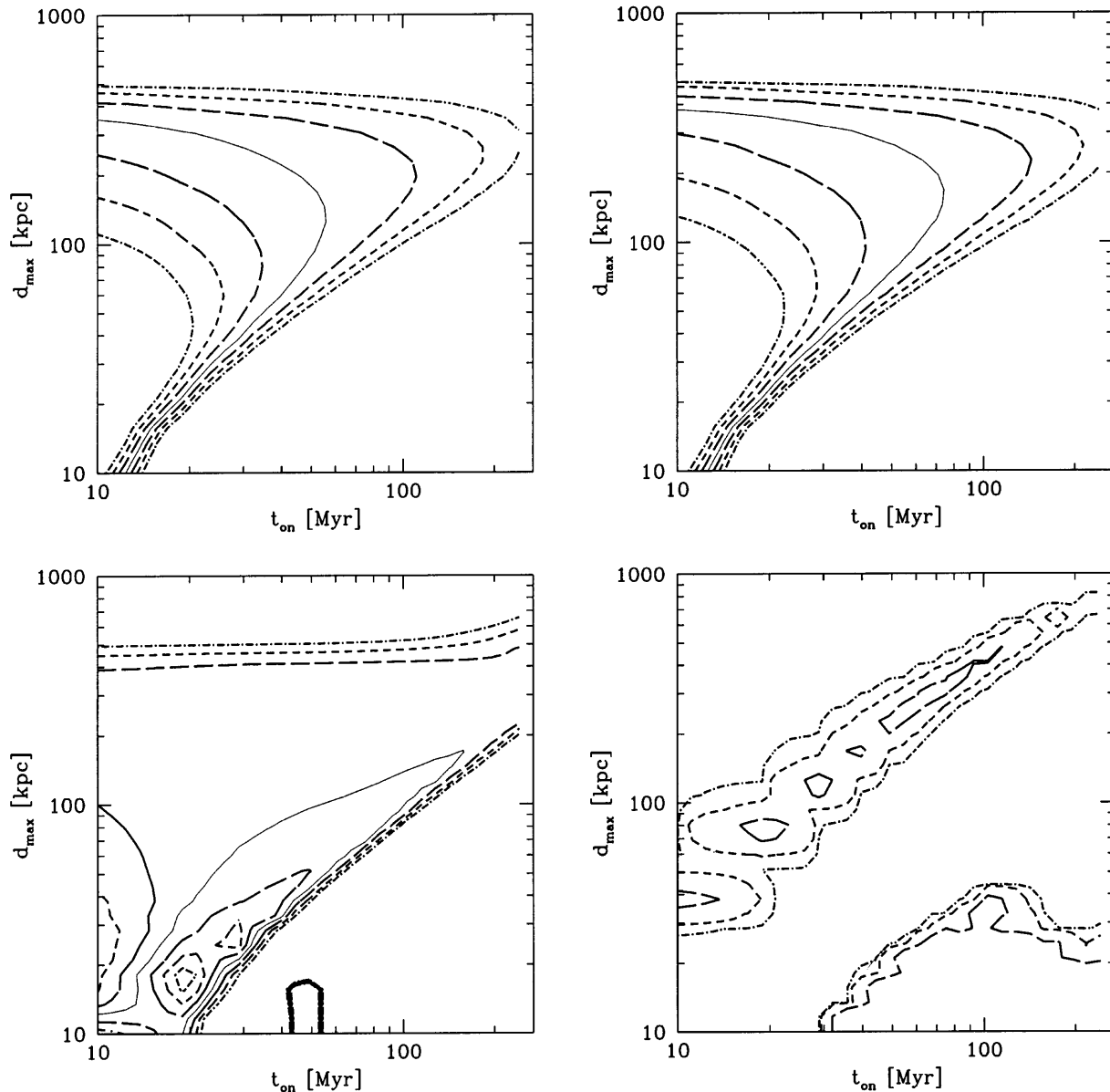


FIG. 5.—Same as Fig. 4, except that the kick velocity  $v_{\text{kick}} = 1000 \text{ km s}^{-1}$

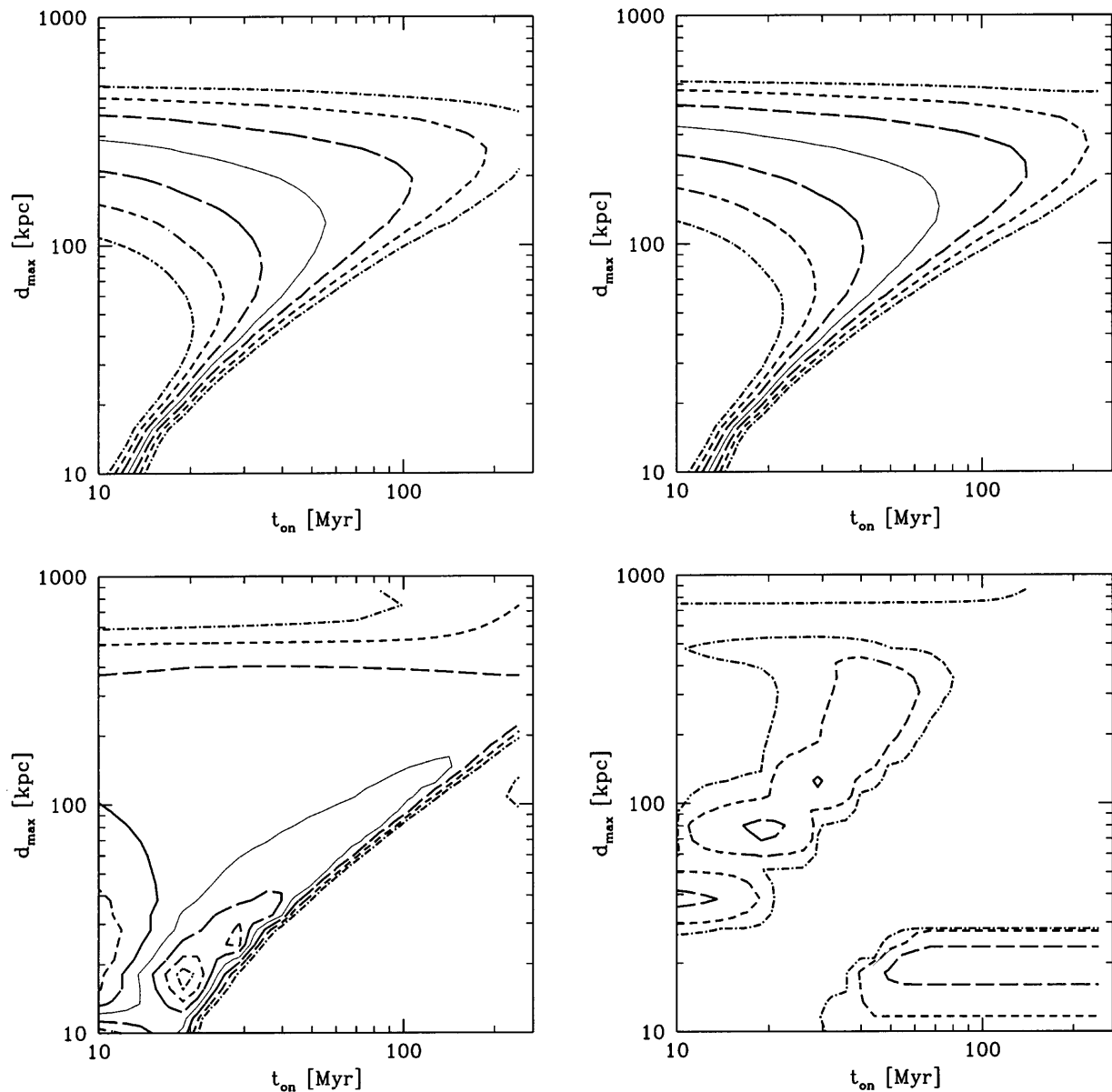


FIG. 6.—Same as Fig. 5, except that the turn-off time  $\Delta T = 2000$  Myr

bursts is similar to that when  $v_{\text{kick}} = 1000 \text{ km s}^{-1}$ . (In the  $v_{\text{kick}} = 2000 \text{ km s}^{-1}$  case, the additional regions that have acceptable dipole moment values for  $t_{\text{on}} > 80$  Myr and  $d_{\text{max}} \approx 100$  kpc are due to neutron stars from M31 passing by through the Galaxy.) However, the space available to match the brightness distribution is not as large; in fact, choosing parameters consistent with isotropy requires parameters only marginally consistent with the burst brightness distribution. This difficulty becomes more severe as the neutron star kick velocity increases. Eventually, the neutron star spatial distribution approaches that of a free-streaming wind, a distribution that is not consistent with the observed burst brightness distribution.

The next parameter that we investigate is the burst luminosity function. We concentrate on the case where the neutron star kick velocity is  $1000 \text{ km s}^{-1}$ . We present the results for a luminosity function width  $w = 10$  in Figure 8 and for a width  $w = 100$  in Figure 10. In both cases, we chose the burst-active phase to be  $\Delta T = 500$  Myr. The most

important conclusion that we draw from these figures is that a broad luminosity function has very little effect. The most visible effects are on the quadrupole moment and the brightness distribution. For the quadrupole moment, the area over which the deviation from the observed value is less than  $1 \sigma$  is larger. This is because of the fact that we see brighter bursts at larger distances, and this compensates for the anisotropy due to bursts originating at small distances. For the same reason, the acceptable values of  $d_{\text{av}}$  in the brightness distribution plot decrease as the width of the luminosity function increases. When the burst-active phase is increased to 2000 Myr, the results are similar (see Figs. 6 and 11). The area over which the deviation from the observed quadrupole moment is acceptable increases. However, it becomes more difficult to accommodate the observed peak flux distribution as the width of the luminosity function increases. This is because more bursts from neutron stars originating in M31 become visible and increasingly distort the faint end of the burst brightness

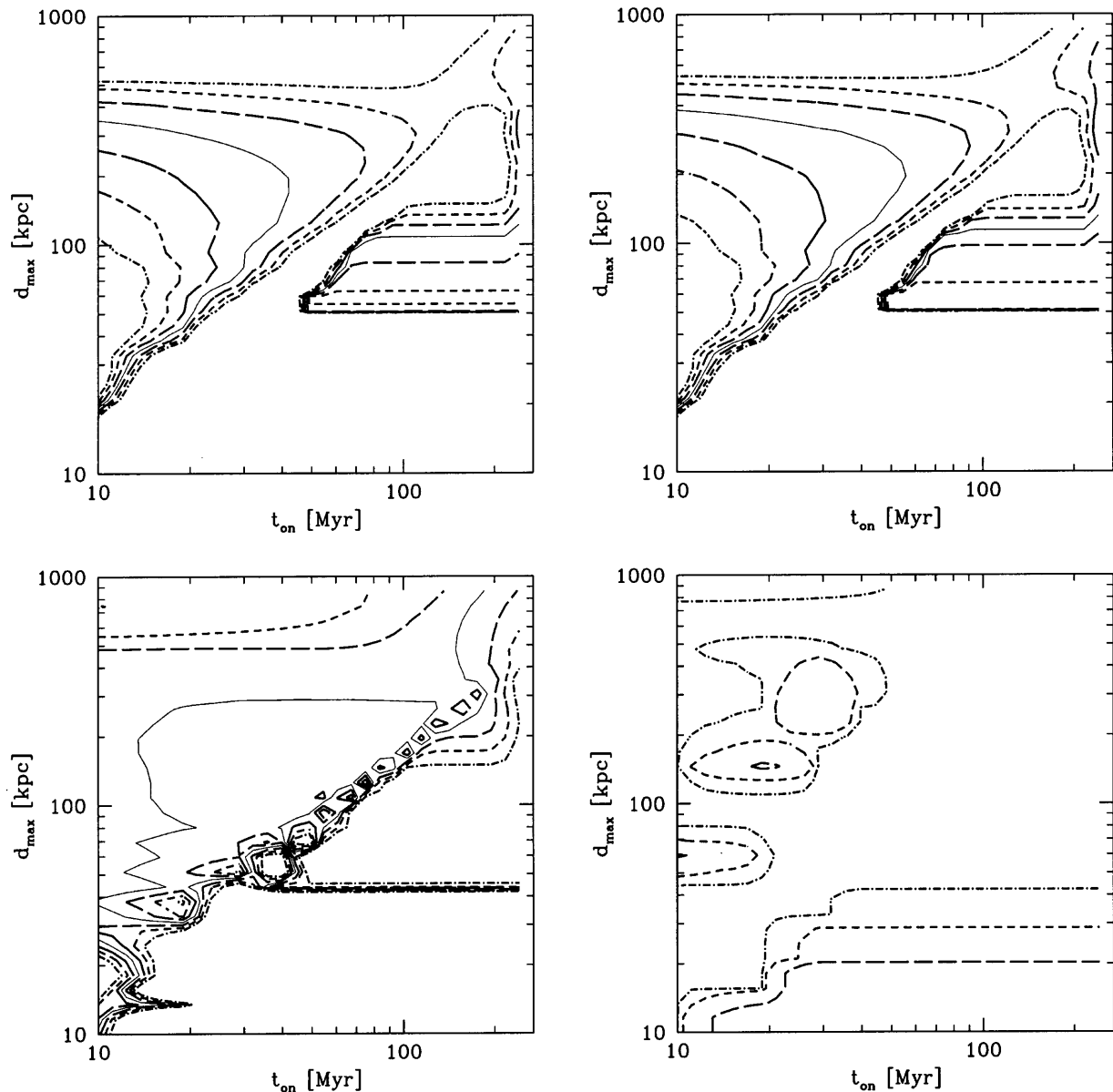


FIG. 7.—Same as Fig. 5, except that the kick velocity  $v_{\text{kick}} = 2000 \text{ km s}^{-1}$  and the turn-off time  $\Delta T = 2000 \text{ Myr}$

distribution. For higher kick velocities, the results are qualitatively similar and show the same general trends.

#### 4.3. Comparison of the Beamed Emission Model with the BATSE Data

In the beamed emission model (Duncan et al. 1993; Li et al. 1994; Li & Duncan 1996a, 1996b; Duncan & Li 1997), the delayed turn-on time parameter  $t_{\text{on}}$  is replaced by the opening half-angle  $\theta_b$  of the beamed emission. Figures 12, 13, and 14 show contour plots for the beamed emission model that are analogous to those for the isotropic emission model with delayed turn-on.

We compare the BATSE data with the expectations of the beamed emission model for a kick velocity  $v_{\text{kick}} = 1000 \text{ km s}^{-1}$  and a burst-active phase of 500 Myr in Figure 12. The region in the lower left corner of the dipole moment plots corresponds to large negative values of the dipole moments because only in the Galactic anticenter direction do we sample beyond the sphere that is empty of visible

bursts. The excluded region on the right ( $d_{\text{max}} < 100 \text{ kpc}$ ,  $\theta_b > 30^\circ$ ) corresponds to a strong positive dipole moment from neutron stars that become visible near their birthplace in the Galactic disk when the beaming cone is wide. Finally, the excluded region in upper part of the plots (large  $d_{\text{max}}$  and small beaming angle) corresponds to an increasing dipole moment toward M31. Although the beamed emission model strongly suppresses visibility of bursts from neutron stars born in M31, the relative contribution of bursts from these neutron stars begins to increase once the BATSE sampling distance exceeds the distance to M31.

In the quadrupole moment plot, we see *two* forbidden regions. For  $d_{\text{max}} > 500 \text{ kpc}$  and  $\theta_b > 30^\circ$ , the large deviation from the BATSE value is due both to the influence of M31 and to the turn-off time. For small beaming angles,  $\theta_b < 15^\circ$ , one encounters a different problem, as illustrated in the top panel of Figure 15. A neutron star that receives a kick perpendicular to the plane of the Galaxy also has a component  $\sim v_{\text{circ}}$  of its net velocity that lies in the disk

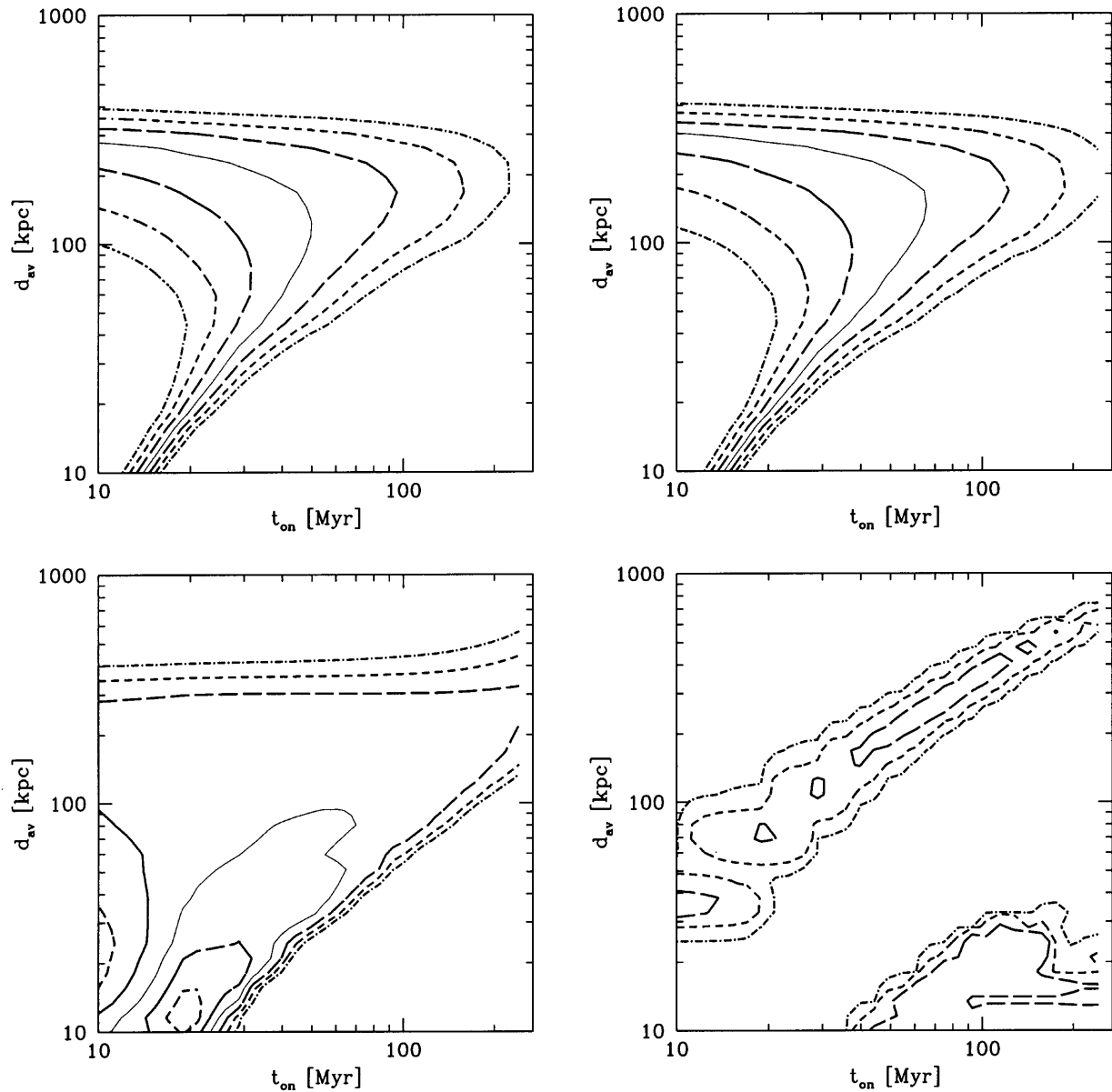


FIG. 8.—Same as Fig. 5, except that the luminosity function has a width of 10, and the comparisons are made in the  $(d_{av}, t_{on})$  plane

plane, corresponding to the rotation velocity of the Galactic disk at its birth location. Thus, for neutron stars that receive a kick velocity perpendicular to the Galactic plane, we never find ourselves in their emission cone and therefore never see them, if the beaming angle is too small. Specifically, in order to see bursts from these neutron stars, the beaming angle must satisfy the condition

$$\theta_B > \tan^{-1} \left( \frac{v_{\text{circ}}}{v_{\text{kick}}} \right); \quad (8)$$

otherwise, there will be a deficit of visible bursts at high Galactic latitudes. We illustrate this in the bottom panel of Figure 15, which shows the burst sky map for a beamed emission model in which  $\theta_b = 8^\circ$ . Thus models that have a small beaming angle require a correspondingly high-kick velocity because of the large quadrupole anisotropy that they would otherwise produce (Fig. 15). Hence, the allowed beaming angles for beamed emission models are bounded from above and below. This has not always been fully

appreciated (but see Li & Duncan 1996a, 1996b; Duncan & Li 1997).

In the figure comparing the model brightness distributions to the BATSE data, the value of  $d_{\text{max}}$  characterizing the allowed region in parameter space rapidly increases and then slowly decreases as  $\theta_b$  increases. We can understand this as follows: For small beaming angles ( $\theta_b < 15^\circ$ ), the sky distribution of bursts resembles that produced by a disk (see Fig. 15), with an angular thickness proportional to the beaming angle. Thus the distance defined by the corresponding break in the brightness distribution increases with increasing beaming angle. Since the ratio of  $d_{\text{max}}$  to the distance of a burst at the break in the burst brightness distribution is fixed by observations, the allowed values of  $d_{\text{max}}$  increase with  $\theta_b$ . For angles larger than  $\theta_b \sim 15^\circ$ , the break in the burst brightness distribution is instead determined by the distance at which we start seeing a substantial fraction of the bursts from our Galaxy. This distance decreases with increasing beaming angle. Since the ratio of  $d_{\text{max}}$  to the typical burst distance at the break is again fixed,

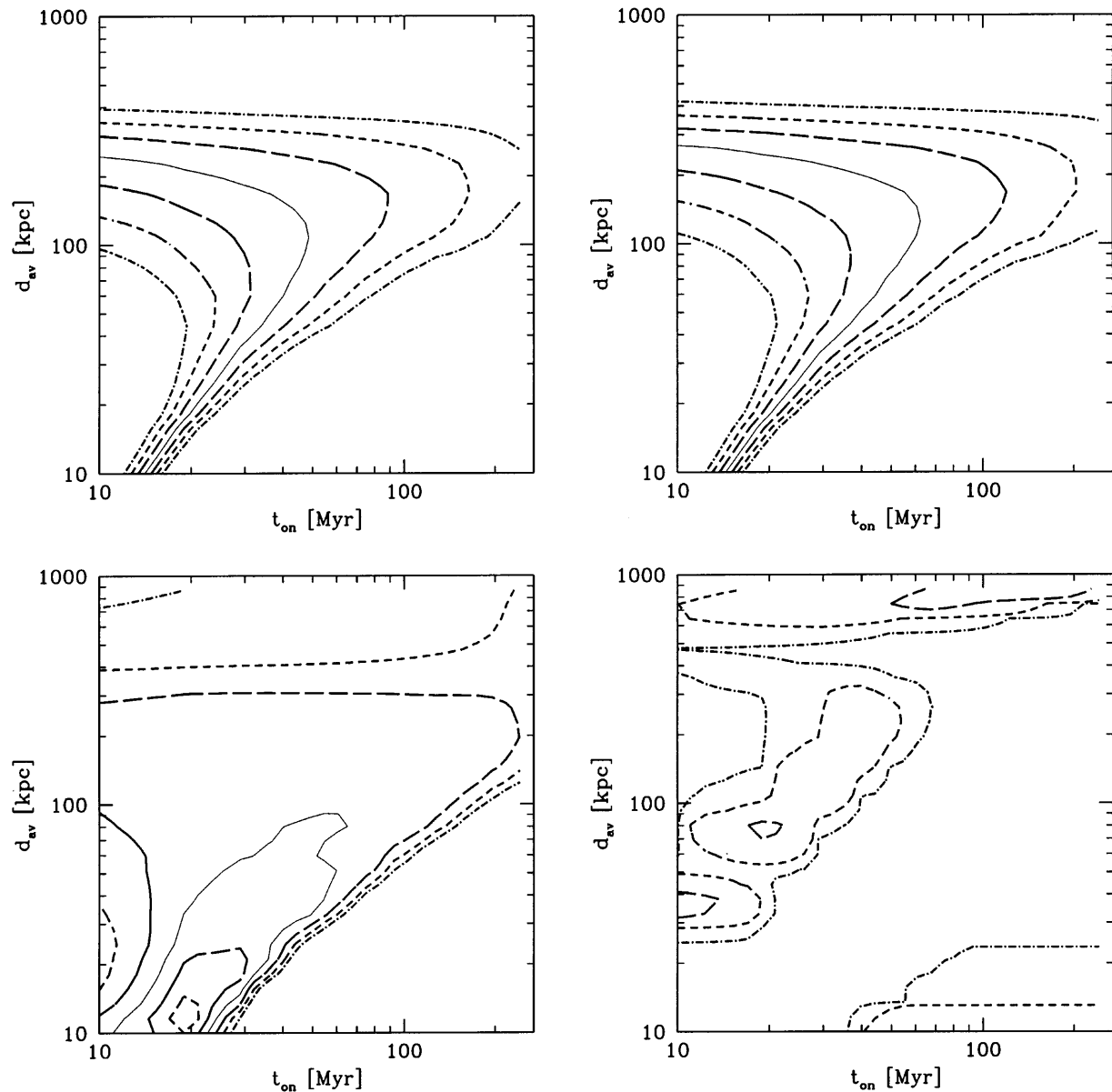


FIG. 9.—Same as Fig. 5, except that the turn-off time  $\Delta T = 2000$  Myr, the luminosity function has a width of 100, and the comparisons are made in the  $(t_{\text{on}}, d_{\text{av}})$  plane.

the allowed values of  $d_{\text{max}}$  now decrease with increasing beaming angle.

In Figure 13, we show the results we obtain when the kick velocity is the same ( $v_{\text{kick}} = 1000 \text{ km s}^{-1}$ ) but the bursting time is increased to 2000 Myr. The main effect of this increase is that the upper limit on  $d_{\text{max}}$  imposed by the observed quadrupole moment increases. (For large beaming angles, this limit is mainly determined by the duration of the burst-active phase.) For completeness, we also show in Figure 14 the results we obtain for a kick velocity of  $1000 \text{ km s}^{-1}$ , a burst-active phase  $\Delta T = 500$  Myr, and a luminosity function with width  $w = 10$ . As in the isotropic emission model with delayed turn-on, a broad luminosity function appears to have little effect; it mainly decreases the allowed average burst distance,  $d_{\text{av}}$ .

#### 4.4. Comparison with the PVO Data

The brightness distribution of the bursts observed by PVO (Ulmer, Wijers, & Fenimore 1995) imposes a very

important constraint on Galactic corona models of GRBs. This brightness distribution is consistent with a power law of slope  $-\frac{3}{2}$ , the value expected for a spatially homogeneous burst distribution. As discussed in Duncan & Li (1997), the beamed emission model naturally explains such a distribution, since the number of bursts visible with increasing distance grows in exactly the right way to mimic a spatially homogeneous distribution. This is not true for the isotropic emission model with delayed turn-on. Models with a burst kick velocity distribution that increases sharply at a velocity  $v_{\text{min}} \gtrsim 800 \text{ km s}^{-1}$  and that have a sharp turn-on at time  $T_{\text{on}}$  always produce a burst spatial distribution with a void at distances less than  $d_{\text{min}} \sim v_{\text{min}} T_{\text{on}}$  and a correspondingly sharp drop in the number of bursts with peak fluxes greater than  $F_{\text{BATSE}}(d_{\text{max}}/d_{\text{min}})^2$ . Consequently, isotropic emission models with a sharp turn-on appear to produce burst brightness distributions that are inconsistent with the PVO data (because the PVO data are not publicly available, we are not able to carry out detailed comparisons

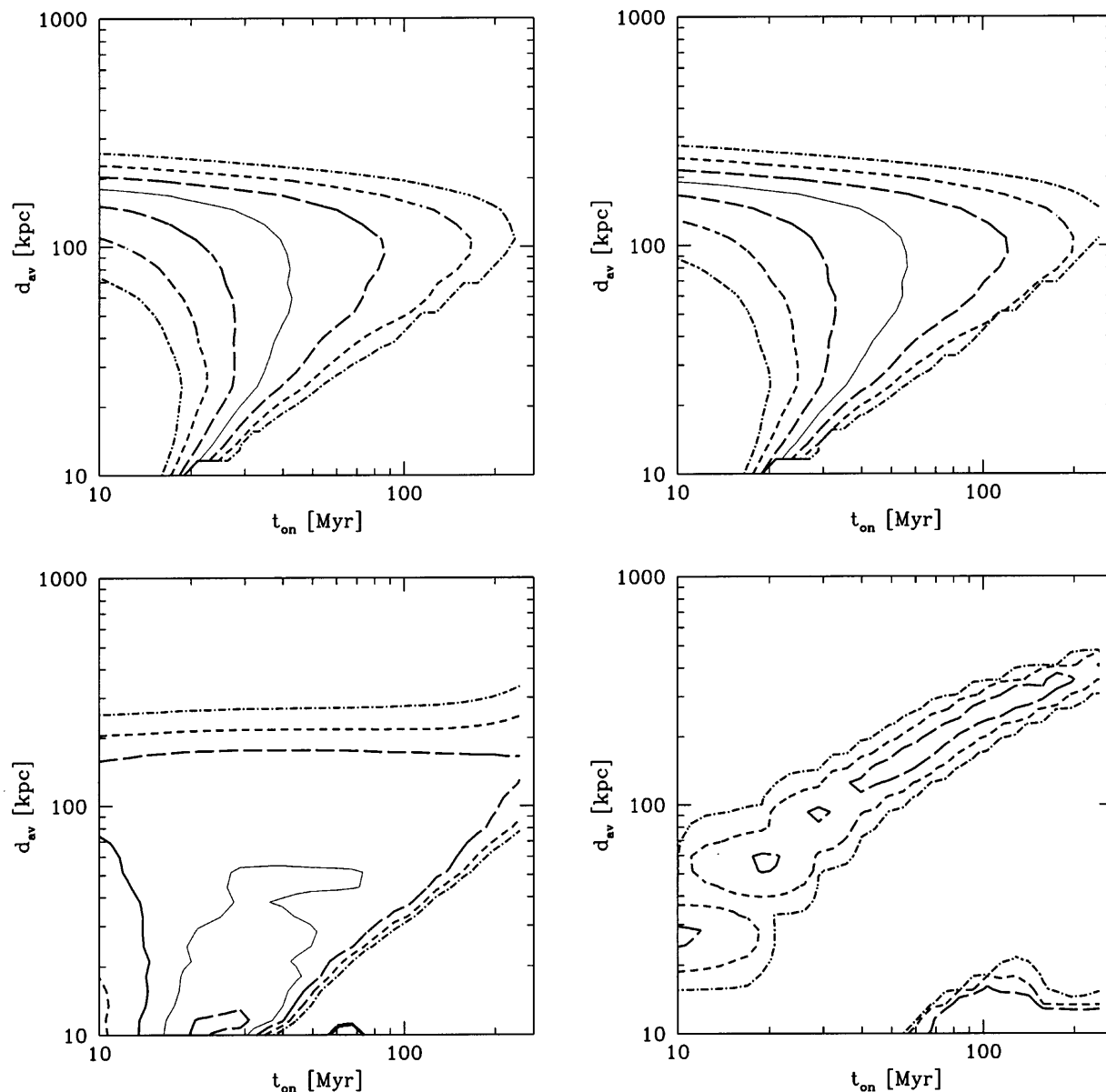


FIG. 10.—Same as Fig. 5, except that the luminosity function has a width of 100, and the comparisons are made in the  $(t_{\text{on}}, d_{\text{av}})$  plane

and therefore rely on fits “by eye” to the published *PVO* burst brightness distribution).

However, there are many effects that tend to remove this sharp drop-off at the bright end of the burst brightness distribution. For example, a spread in kick velocities above  $v_{\text{min}}$  smooths out the edge of the void in the spatial distribution of bursts and therefore smooths out the sharp drop-off in the brightness distribution. A second possibility is that the bursting rate does not increase abruptly at  $t_{\text{on}}$ . In Figure 16, we show the brightness distribution produced by a model (that is consistent with the dipole and quadrupole moments derived from the BATSE data) in which the burst rate initially grows as  $t^2$  and asymptotes to a constant value for times  $t \gtrsim t_{\text{on}} = 30$  Myr. This model produces a brightness distribution that agrees well with both the BATSE and the *PVO* burst brightness distributions. A third effect that will tend to smooth out the sharp drop-off in the brightness distribution (and one that almost certainly exists) is a moderately broad burst luminosity function. A width  $w \gtrsim 10$  in

the luminosity function produces a  $-\frac{3}{2}$  slope at the high end of the burst brightness distribution for a fairly wide range of model parameters. As an illustration of this, we also show in Figure 16 the brightness distribution obtained for a sharp turn-on model and  $w = 10$ . Again, the agreement with both the BATSE and the *PVO* burst brightness distributions is reasonably good. A rigorous likelihood analysis of the BATSE data (Loredo & Wasserman 1998a, 1998b) shows that the width  $w$  of the burst luminosity function is currently *not* well constrained. In fact, one can consider the results presented here as proof by construction that the BATSE data are consistent with a broad burst luminosity function. Finally, we note that, if the burst active phase lasts for longer than  $\sim 1$  Gyr, neutron stars born in M31 have time to propagate to the inner parts of our Galaxy (see also Podsiadlowski et al. 1995). In models with  $\Delta T \gtrsim 2$  Gyr, there is always a significant number of neutron stars in the inner parts of our Galaxy that were born in M31 and that produce bursts, which tends to

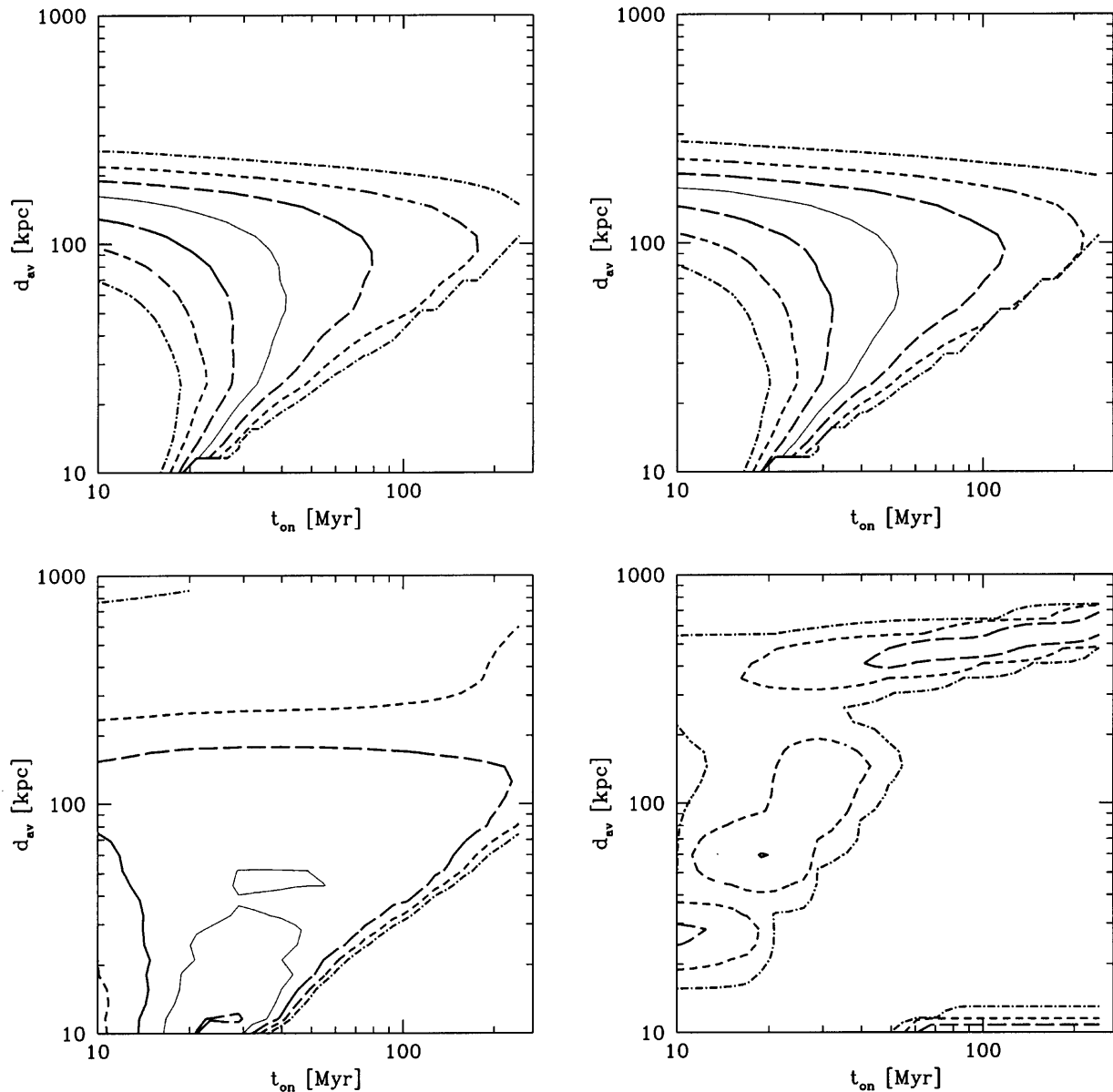


FIG. 11.—Same as Fig. 5, except that the turn-off time  $\Delta T = 2000$  Myr, the luminosity function has a width of 100, and the comparisons are made in the  $(t_{\text{on}}, d_{\text{av}})$  plane.

smooth out the sharp drop-off in the brightness distribution (although there are not enough for this effect alone to explain the  $-\frac{3}{2}$  slope).

##### 5. THE ROLE OF M31

The inclusion of M31 in corona models has two main effects. First, M31 represents an additional source of bursts that originate from the same point on the sky. If BATSE or another instrument were to see sufficiently far toward M31, an excess of bursts in the direction of M31 should become readily apparent (e.g., as in Fig. 1 of Bulik et al. 1996). In the isotropic emission model, the lack of such an excess in the BATSE data sets a firm upper limit on the current BATSE sampling distance,  $d_{\text{max}}$ : as the study quoted above shows, the expected sky distribution becomes highly anisotropic once an instrument sees beyond  $\sim 400$  kpc, about two-thirds of the distance to M31 ( $d_{\text{M31}} = 640$  kpc).

In contrast, in the beamed emission model, most of the neutron stars escaping our Galaxy eventually become

visible, while only a small fraction of the neutron stars born in M31 are ever seen. This fraction is  $\sim \Delta\Omega_{\text{beam}}/4\pi$ , where  $\Delta\Omega_{\text{beam}}$  is the beaming solid angle (however, as discussed above, the beaming solid angle cannot be arbitrarily small). Thus the excess of bursts seen in the direction of M31 can be made small, as long as the instrument is unable to see beyond M31 (see also Duncan & Li 1997).

The second, more subtle effect that M31 has is to distort the shape of the neutron star corona. Neutron stars from our Galaxy that pass near M31 are accelerated and deflected toward M31 as they approach M31, then decelerated once they have passed M31, and then begin to climb out of its potential well. As noted in Podsiadlowski et al. (1995), this produces an excess or “hot spot” of bursts behind M31 due to neutron stars that are born in our Galaxy and are focused behind M31; and by symmetry, a similar hot spot of bursts exists in the direction opposite M31 due to neutron stars that are born in M31 and that are focused behind our Galaxy (Coppi et al. 1996). Also,

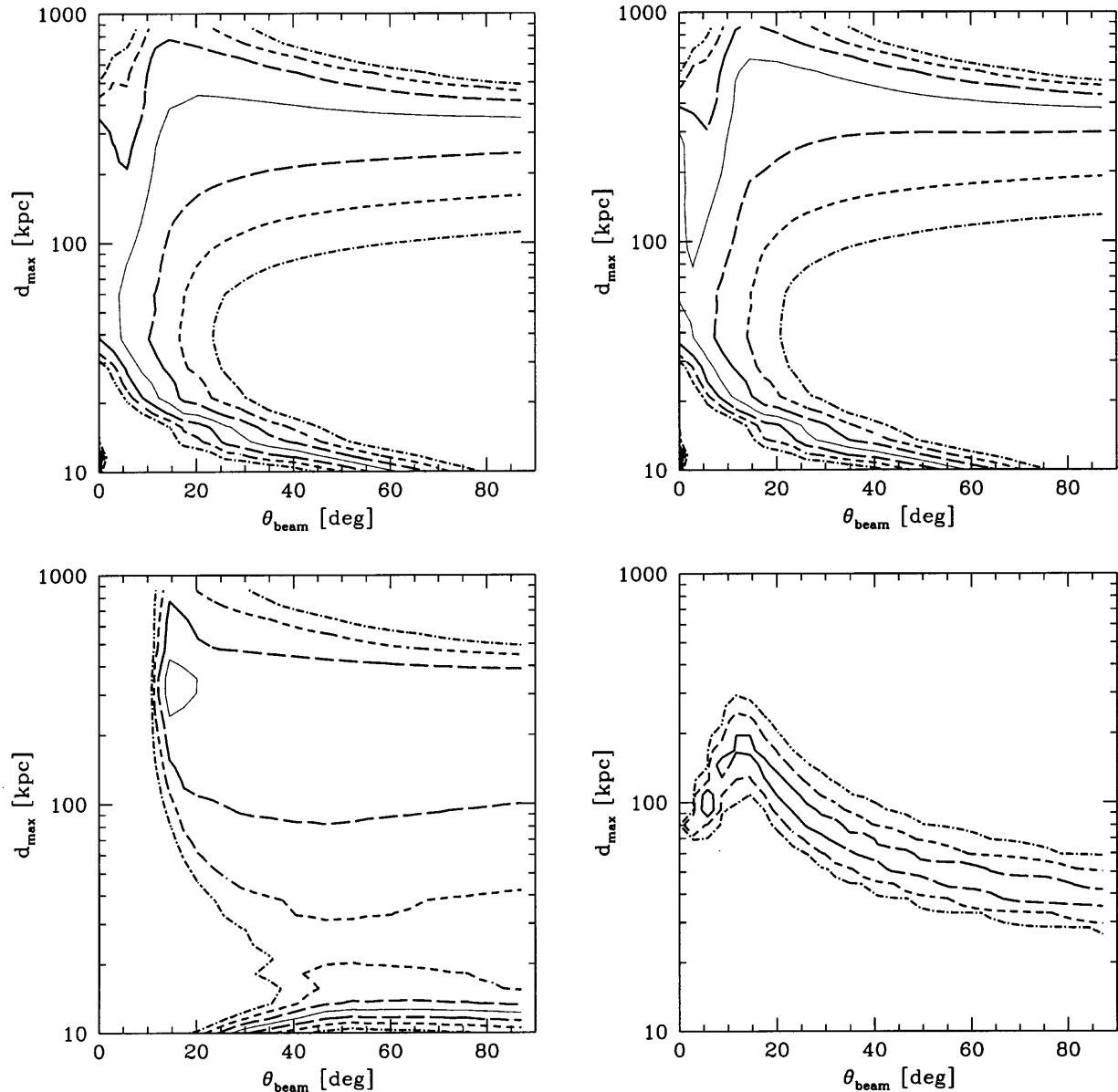


FIG. 12.—Comparison between the Galactic dipole moment (*upper left*), the dipole moment relative to M31 (*upper right*), the Galactic quadrupole moment (*lower left*), and the distribution of burst peak fluxes (*lower right*) derived from the BATSE data and those expected in the beamed emission model for a kick velocity  $v_{\text{kick}} = 1000 \text{ km s}^{-1}$ , a turn-off time  $\Delta T = 500 \text{ Myr}$ , and a luminosity function of zero width, in the  $(\theta_b, d_{\text{max}})$  plane. The contours in the first three panels delineate the regions within which the model deviates from the BATSE values by less than  $1 \sigma$  (*long-dashed line*),  $2 \sigma$  (*short-dashed line*), and  $3 \sigma$  (*dash-dotted line*); along the thin solid lines, the model has the exact value derived from the BATSE 3B data. The contours in the fourth panel delineate the regions within which the BATSE data and the model are consistent at the 32%, 5%, and 0.4% probability levels.

because the mass of our Galaxy and the mass of M31 are comparable, the outer corona surrounding the combined Milky Way–M31 system is significantly more compact than it would be in the case of the Milky Way alone; i.e., M31 significantly changes the brightness distribution of bursts originating  $\gtrsim 400 \text{ kpc}$  from us. Finally, as emphasized by Podsiadlowski et al. (1995), the inclusion of M31 breaks the overall circular and spherical symmetries of the gravitational potential and leads to bound neutron star orbits that are typically neither periodic nor closed. In particular, we have verified that bound stars returning to our Galaxy at late times do not show a strong disklike signature, despite having been born in the disk of our Galaxy.

While M31 has significant dynamical effects on the neutron stars in the corona, in general these effects do *not* play an important role if one restricts one's attention to

sampling distances consistent with the BATSE data, i.e.,  $d_{\text{max}} \lesssim 400 \text{ kpc}$ . The one exception is when the burst-active phase lasts longer than  $\sim 1 \text{ Gyr}$ . This is enough time for bound neutron stars born in our Galaxy to begin to return and for unbound neutron stars born in M31 to begin to reach us.

## 6. DISCUSSION

### 6.1. Constraints on Parameters of the Galactic Corona Model

We have examined a large range of parameter values for both isotropic emission models with delayed turn-on and beamed emission models, within the framework of the Galactic corona model. Since the velocity distribution of neutron stars is uncertain, we have used a Green's function-type approach to examine the dependence of Galactic



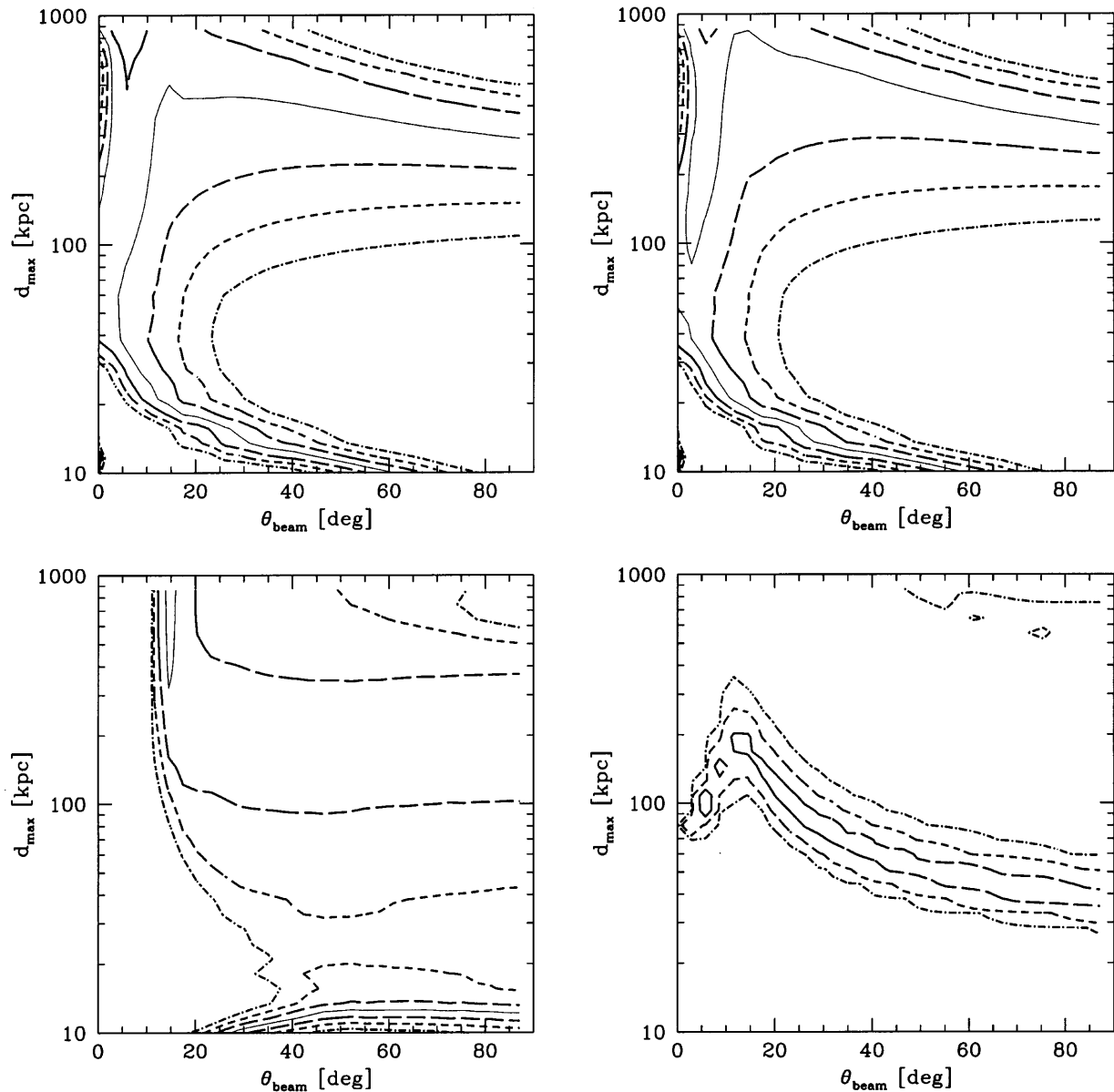


FIG. 13.—Same as Fig. 12, except that  $\Delta T = 2000$  Myr

corona models on kick velocity. We find that the parameter space for the models opens up significantly when most of the bursting neutron stars are only weakly bound or unbound in the Galactic potential. This sets a lower limit on the kick velocity of bursting neutron stars of  $\sim 800 \text{ km s}^{-1}$ . On the other hand, when the kick velocity becomes very large ( $\geq 2000\text{--}3000 \text{ km s}^{-1}$ ), the spatial distribution of the neutron stars in the corona approaches that of a free-streaming wind from our Galaxy, a distribution that is not consistent with the observed BATSE brightness distribution.

Two requirements must be satisfied in order to avoid a strong Galactic anisotropy signature. First, the typical distance out to which we can see bursts must be large compared to the Sun's distance from the Galactic center. This requires sampling distances  $\geq 130$  kpc for isotropic emission models and  $\geq 80$  kpc for beamed emission models. Second, no matter what the neutron star kick velocities, the component of bursts due to young neutron stars always shows a significant Galactic dipole and quadrupole

moment, because young stars lie too close to their birthplaces, which are presumably near the Galactic disk. To meet the BATSE data constraints, we must therefore not see bursts from young neutron stars. For isotropic emission models, this imposes a lower limit on the typical age at which a significant fraction of neutron stars begin to burst, namely,  $t_{\text{on}} > 20$  Myr for  $v_{\text{kick}} = 1000 \text{ km s}^{-1}$ . In the case of beamed emission models, the same requirement imposes an upper limit on the beaming angle  $\theta_b < 25^\circ$ . At the same time, we find that the beaming angle cannot be made arbitrarily small, since small beaming angles produce a very strong quadrupole anisotropy, in agreement with the results of Duncan & Li (1997). For kick velocities  $\sim 1000 \text{ km s}^{-1}$ , we find that the beaming angle must be  $\theta_b \geq 15^\circ$ .

The duration,  $\Delta T$ , of the burst-active phase must be longer than a few hundred Myr so that neutron stars have time to propagate well beyond the allowed BATSE sampling distance. However, the observed isotropy and burst brightness distribution do not seem to constrain strongly the duration of the burst-active phase from above. For long

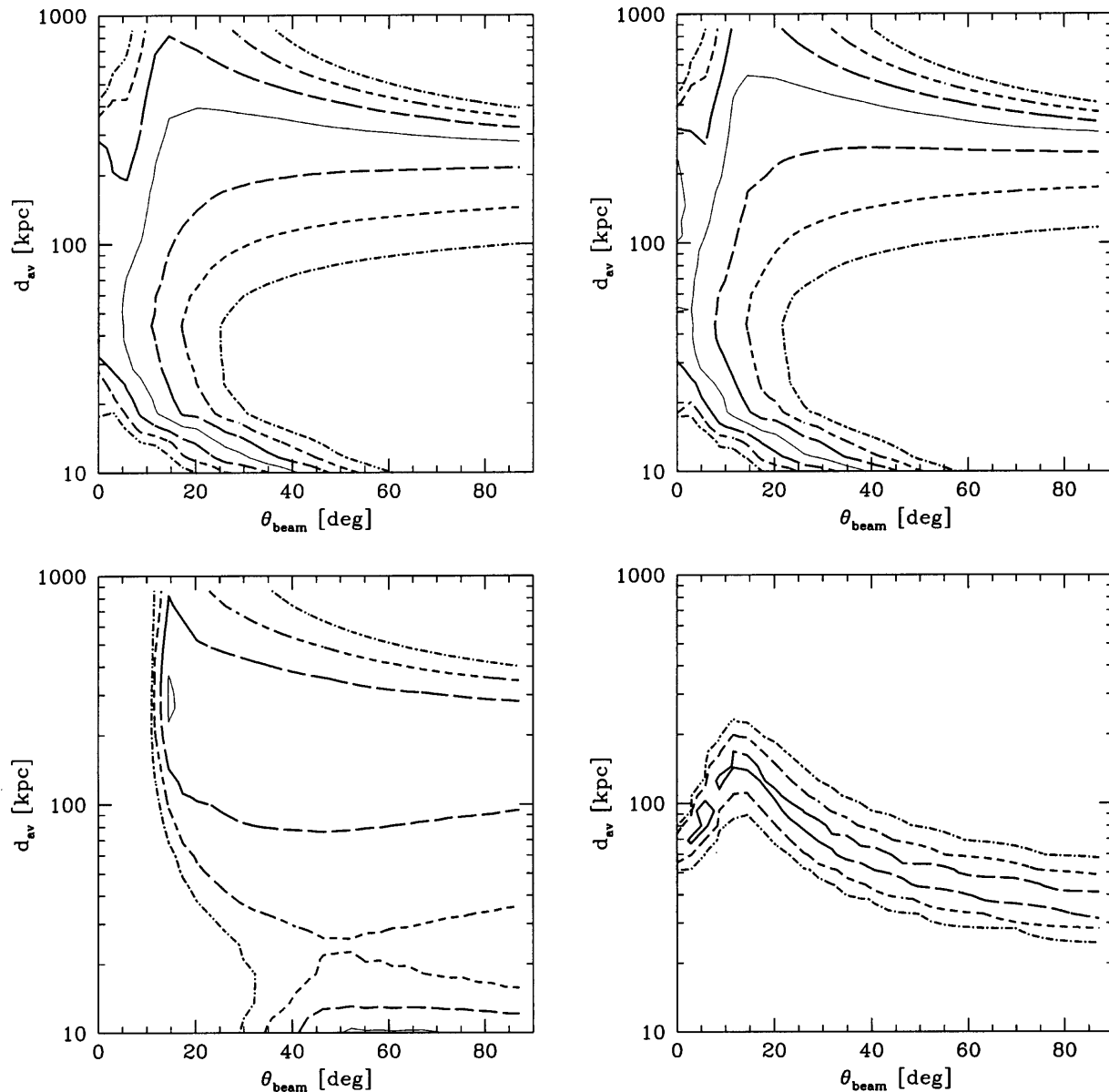


FIG. 14.—Same as Fig. 12, except that the luminosity function has a width of 100

burst-active phases, some stars from M31 have time to begin to reach us, and also the fraction of the neutron stars born in our Galaxy that are bound have time to begin to return. However, for the kick velocities considered here, the number of such old stars in our Galaxy is relatively small. Also, because of the asymmetry of the combined gravitational potential of the Milky Way and M31, we find that the resulting neutron star distribution does not show a significant Galactic signature, even for burst active phases and propagation times as long as  $\Delta T = 9$  Gyr, in agreement with the results of Podsiadlowski et al. (1995). In general, longer burst-active phases appear to be slightly more difficult to reconcile with the BATSE brightness distribution, but they help with matching the slope of the *PVO* brightness distribution.

The width  $w$  of the burst luminosity function appears to be practically unconstrained by the BATSE data. Values of  $w$  from 1–100 are consistent with the dipole moments, the quadrupole moment, and the brightness distribution of the

BATSE bursts, and the allowed parameter regions do not depend on  $w$ . This is true for both isotropic emission and beamed emission models. However, for isotropic emission models with delayed turn-on, the width of the luminosity function must be  $w \gtrsim 10$  in order to match the *PVO* brightness distribution, if the bursting turns on sharply. The *PVO* brightness distribution can also be explained by a range of kick velocities above the minimum value or by a gradual increase in the initial rate of bursting.

The upper limit on the BATSE sampling distance (or, equivalently, the lower limit on the burst peak flux) is imposed by either the duration of the burst active phase, if it is shorter than 500 Myr, or by the presence of M31, which acts as an additional source of bursts. In the case of the isotropic emission model with delayed turn-on, the upper limit is about 400 kpc. In the beamed emission model, the number of bursts from M31 is typically strongly suppressed. Hence the upper distance is constrained mainly by the brightness distribution, which gives  $d_{\max} \lesssim 250$  kpc.

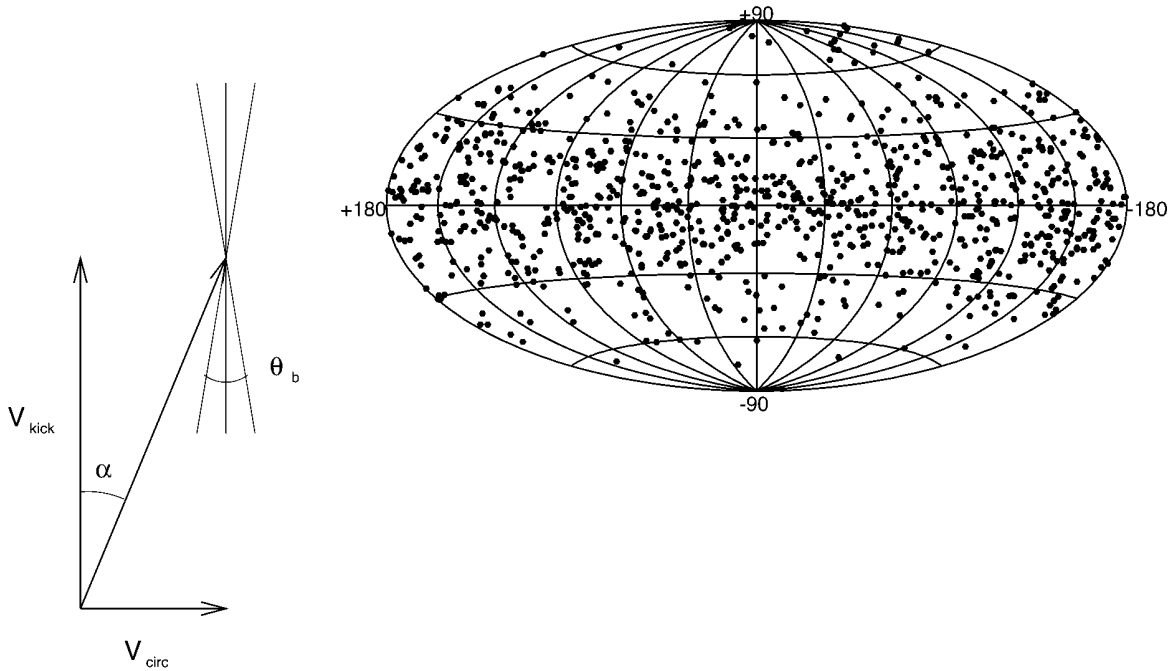


FIG. 15.—*Left*: Origin of the lower limit on the beaming angle  $\theta_b$ . A neutron star with the kick velocity  $V_{\text{kick}}$  perpendicular to the disk plane also has a galactic circular velocity  $V_{\text{circ}}$  in the plane. However, its bursts are beamed parallel and antiparallel to the direction of  $V_{\text{kick}}$ . Consequently, if the angle  $\alpha \equiv v_{\text{circ}}/v_{\text{kick}}$  is larger than  $\theta_b$ , an observer in the Galaxy near the place where the neutron star was born will never see bursts from this neutron star, leading to a paucity of bursts at high Galactic latitudes. This is illustrated in the right panel, which shows the resulting sky map for  $v_{\text{kick}} = 1000 \text{ km s}^{-1}$ ,  $d_{\text{max}} = 200 \text{ kpc}$ ,  $\Delta T = 500 \text{ Myr}$ , and  $\theta_b = 8^\circ$ .

### 6.2. The Role of the Rotational Velocity of the Galaxy Disk

In calculating the spatial distribution of the neutron stars in the Galactic corona, it is essential to include the rotational velocity of the Galactic disk. As we showed in § 3, assuming that the neutron star kick velocity is random in the frame locally corotating with the disk significantly alters the distribution of neutron stars in the Galactic corona. In particular, the distribution of neutron stars of a given kick velocity and age *cannot* be approximated by a spherical shell, as assumed, e.g., by Hartmann, Greiner, & Briggs (1995). To verify this, we have performed a calculation in which the effects of the rotational velocity of the Galactic disk were “turned off.” The parameter space that is consistent with the BATSE data shrank very significantly.

### 6.3. Anisotropy as a Function of Brightness

A possible signature of high-velocity neutron star corona models of GRBs is anisotropy as a function of brightness, similar to that in the BATSE 1B catalog reported by Quashnock & Lamb (1993). In Figure 17, we show examples of the expected dipole and quadrupole moments as a function of peak flux. The kick velocity is  $1000 \text{ km s}^{-1}$  and the results are shown for three turn-on times:  $t_{\text{on}} = 20, 30,$  and  $100 \text{ Myr}$ . At high burst peak fluxes, the curves are dominated by numerical noise. While the curves show a definite pattern for each model, it is difficult to make robust, quantitative predictions. In addition, a spread in kick velocities, a moderately wide luminosity function, or a gradual (rather than an abrupt) bursting turn-on will smooth out the curves. While detection of an anisotropy as a function of burst brightness would constitute a confirmation of the Galactic corona models, the lack of such a detection can probably be accommodated within the models

presented above when these possible effects are taken into account.

One can use the contour plots (Figs. 5–14) to read off the expected anisotropy as a function of brightness for a particular model. This can be done by fixing either the turn-on time  $t_{\text{on}}$  in isotropic emission models or the beaming angle  $\theta_b$  in beamed emission models and then recording the size of the dipole and quadrupole moments as one varies either the sampling distance  $d_{\text{max}}$  or the distance to an average burst  $d_{\text{av}}$ . As an example, we see from Figure 8 that for  $t_{\text{on}} = 40 \text{ Myr}$ , the deviations of the dipole and quadrupole moments from the BATSE values are smaller than  $1 \sigma$  over a factor of 10 in distance. This corresponds to 2 orders of magnitude in burst peak flux. Thus the expected anisotropy as a function of burst brightness can be quite small over the BATSE range of burst peak fluxes. However, all of the models predict some signature of anisotropy for very bright and very dim bursts (see, e.g., Fig. 8, *top panel*).

### 6.4. Burst Energetic Requirements and Repetition Rate

We have shown that a distant Galactic corona of high-velocity neutron stars can simultaneously reproduce the observed isotropy of GRBs and their peak flux distribution. Here we consider the burst energy and repetition rate requirements of such a model.

We take  $F_{\text{peak}} \sim 10^{-7} \text{ ergs cm}^{-2} \text{ s}^{-1}$  as the typical peak energy flux of a BATSE burst. Then the typical burst luminosity is

$$L_{\text{burst}} \approx 10^{41} \left( \frac{F_{\text{peak}}}{10^{-7} \text{ ergs cm}^{-2} \text{ s}^{-1}} \right) \left( \frac{d}{100 \text{ kpc}} \right)^2 \text{ ergs s}^{-1}. \quad (9)$$

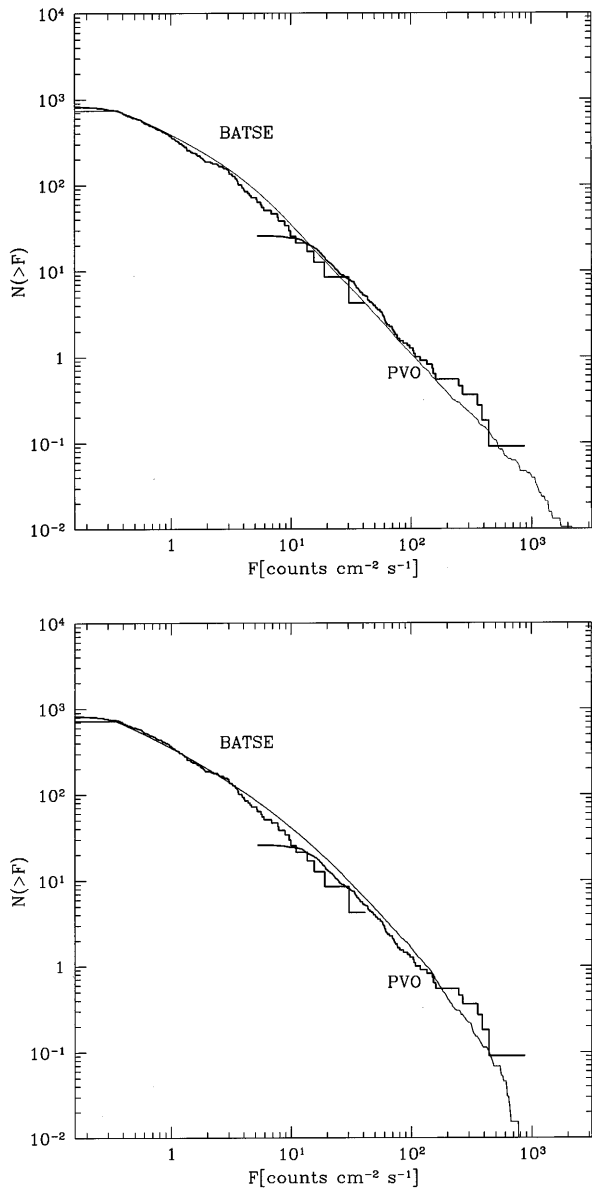


FIG. 16.—Comparison of the cumulative peak flux distributions derived from the BATSE 3B catalog and the PVO data (*thick solid lines*) and those expected in the isotropic emission model (*thin solid lines*). The top panel shows the cumulative peak flux distribution expected in the isotropic emission model for  $v_{\text{kick}} = 1000 \text{ km s}^{-1}$ ,  $\Delta T = 500 \text{ Myr}$ , a luminosity function of zero width, and a burst rate increasing like  $t^2$  for a period of 50 Myr and then remaining constant. The bottom panel shows the cumulative peak flux distribution expected in the isotropic emission model for  $v_{\text{kick}} = 1000 \text{ km s}^{-1}$ ,  $\Delta T = 500 \text{ Myr}$ , a burst rate increasing suddenly from zero to a constant value at a time (age)  $t_{\text{on}} = 30 \text{ Myr}$ , and a luminosity function of width  $w = 10$ .

Taking 5 s as the average photon flux-to-energy flux conversion factor for BATSE bursts (Fenimore et al. 1993), the typical burst energy is then

$$E_{\text{burst}} \approx 5 \times 10^{41} \left( \frac{F_{\text{peak}}}{10^{-7} \text{ ergs cm}^{-2} \text{ s}^{-1}} \right) \left( \frac{d}{100 \text{ kpc}} \right)^2 \text{ ergs} . \quad (10)$$

The rate of burst detection by BATSE corresponds to an all-sky rate  $R_{\text{burst}}^{\text{BATSE}} \sim 800 \text{ bursts yr}^{-1}$ . Assuming a neutron star birth rate  $R_{\text{NS}} \sim 3 \times 10^{-2} \text{ yr}^{-1}$ , the total number of

bursts that each neutron star must produce during its burst-active phase is

$$N \approx \frac{R_{\text{burst}}^{\text{BATSE}}}{(f_{\text{escape}} R_{\text{NS}})} \approx 8 \times 10^4 \left( \frac{f_{\text{escape}}}{0.3} \right)^{-1} , \quad (11)$$

where  $f_{\text{escape}}$  is the fraction of neutron stars born with velocities high enough to escape from the Galaxy. Equation (11) implies that, on average, high-velocity neutron stars burst at least once every  $\sim 10^3 \text{ yr}$ . The total supply of energy needed by each high-velocity neutron star in the Galactic corona is then

$$E \approx N \left( \frac{E_{\text{burst}}}{5 \times 10^{41}} \right) \approx 4 \times 10^{46} \text{ ergs} . \quad (12)$$

Possible energy sources include gravitational energy from accretion of planetesimals (Colgate & Leonard 1993; Woosley 1993) and magnetic field energy stored in the interior of the neutron star (Podsiadlowski et al. 1995). For a more extensive discussion of these possibilities, see Lamb (1995), Lamb et al. (1996), and references therein.

## 7. CONCLUSIONS

We have attempted to survey the parameter space available to high-velocity neutron star Galactic corona models. Provided that the typical neutron star kick velocities are sufficiently large, we conclude that the parameter space allowed by current data is surprisingly large. In this sense, corona models are robust and do not require fine-tuning. The requirement for high neutron star kick velocities can be met in two ways: either a very large fraction of neutron stars must have such velocities, or there must be a connection between the bursting properties of a neutron star and its kick velocity.

We have shown that the angular distribution of bursts produced by a distant Galactic corona of high-velocity neutron stars can be remarkably isotropic. For example, the model shown in Figure 8 with  $t_{\text{on}} = 100 \text{ Myr}$  and  $d_{\text{av}} = 170 \text{ kpc}$  has expected dipole and quadrupole moments of  $\langle \cos \theta \rangle = 0.0033$  and  $\langle \sin^2 b - \frac{1}{3} \rangle = -0.0046$ , after correcting for the BATSE sky exposure. These values are extremely small and would require more than a decade of continued BATSE observations in order to rule them out. The most significant isotropy constraints on Galactic corona models are likely to come not from the isotropy of all bursts, but from limits on the isotropy of the brightest ones. As shown in Figure 17, all Galactic corona models predict some anisotropy as a function of burst brightness, especially for the brightest bursts. (The details depend on the exact model, however.) We remark that, if Galactic bursts constitute only a fraction of all bursts, then the constraints presented here are correspondingly relaxed. For example, much lower neutron star kick velocities might be allowed if their Galactic signal is diluted by an isotropic population of cosmological bursts.

Because Galactic corona and cosmological models of GRBs can produce remarkably similar angular and brightness distributions, the best way to confirm or reject the Galactic corona models probably does not lie in further constraining the isotropy or the brightness distribution of the bursts. Rather, one should probably seek other signatures that might unequivocally distinguish between the two possibilities. The future of the GRB field almost certainly lies in the direction of determining burst locations very

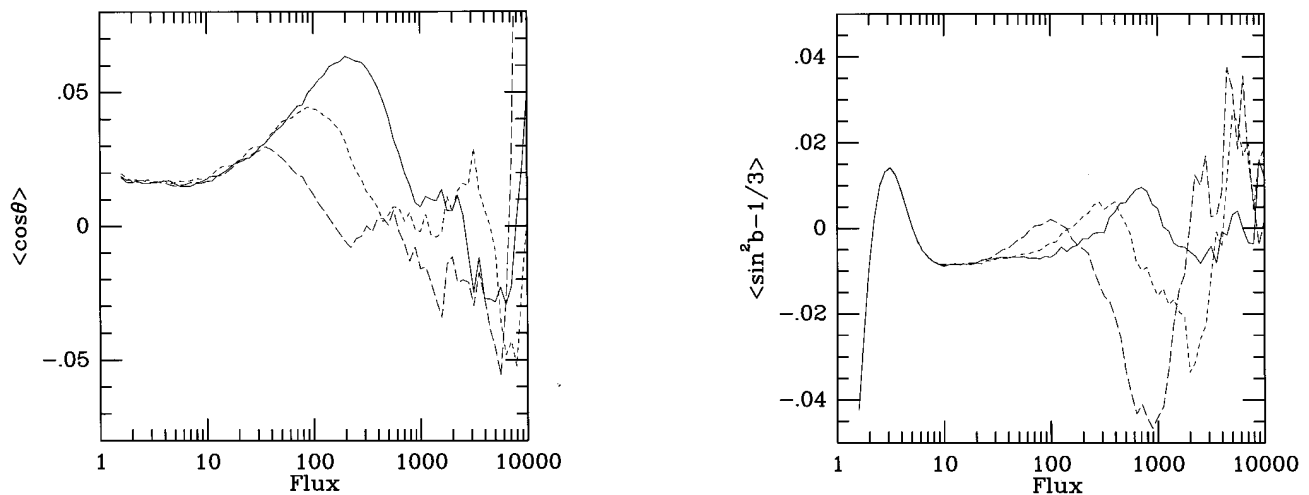


FIG. 17.—Expected Galactic dipole moment (*left*) and Galactic quadrupole moment (*right*) as a function of burst peak flux in arbitrary units, for a sliding window in flux with a logarithmic width of 0.3 (the size of the sliding window used by Quashnock & Lamb 1993 in their analysis of the BATSE 1B catalog) for the model parameters of Fig. 5 and three values of the turn-on time  $\delta t = 20$  Myr (*solid line*),  $\delta t = 30$  Myr (*short-dashed line*), and  $\delta t = 50$  Myr (*long-dashed line*).

accurately and disseminating them rapidly to the worldwide astronomical community, so that rapid and sensitive counterpart searches can be made (consider the impact that just a few *BeppoSAX* localizations have had). For example, accurate locations would either confirm or severely constrain burst repetition, clarify the severity of the “no-host problem” (Schaefer 1992; Schaefer et al. 1998), and determine the characteristics of bursts showing afterglows or violating the X-ray–paucity constraint. As a second example, a sufficiently sensitive instrument with good positional resolution could directly detect bursts from a corona around M31, if the majority of BATSE bursts indeed come

from a Galactic corona (Li, Fenimore, & Liang 1996; Coppi et al. 1996). Finally, significant advances could also come from improving the spectral resolution of wide-angle burst detectors. This would enable comprehensive, sensitive searches for spectral features, i.e., cyclotron scattering lines, which might be characteristic of the physics of a particular class of bursts.

This research was supported in part by NASA grants NAG5-2868, NAG5-1454, NASW-4690 and by KBN grant 2P03D00911. This work has made use of NASA’s Astrophysics Data System Abstract Service.

#### REFERENCES

- Binney, J., & Tremaine, S. 1987, *Galactic Dynamics* (Princeton: Princeton Univ. Press)
- Blaes, O., & Madau, P. 1993, *ApJ*, 403, 690
- Briggs, M. S., Band, D. L., Preece, R. D., Pendleton, G. N., Paciesas, W. S., Ford, L., & Matteson, J. L. 1996, in *AIP Conf. Proc. 384, Gamma-Ray Bursts*, ed. C. Kouveliotou, M. S. Briggs, & G. J. Fishman (New York: AIP), 153
- Briggs, M. S., Band, D. L., Preece, R. D., Pendleton, G. N., Paciesas, W. S., & Matteson, J. L. 1998, in *Proc. 4th Huntsville Symp., Gamma-Ray Bursts*, ed. C. Meegan & R. Preece (New York: AIP), in press
- Bulik, T., Coppi, P. S., & Lamb, D. Q. 1996, in *AIP Conf. Proc. 384, Gamma-Ray Bursts*, ed. C. Kouveliotou, M. S. Briggs, & G. J. Fishman (New York: AIP), 340
- Bulik, T., & Lamb, D. Q. 1995, *Ap&SS*, 231, 373
- . 1996a, in *AIP Conf. Proc. 366, High-Velocity Neutron Stars and Gamma-Ray Bursts*, ed. R. E. Rothschild & R. E. Lingenfelter (New York: AIP), 258
- . 1996b, in *AIP Conf. Proc. 384, Gamma-Ray Bursts*, ed. C. Kouveliotou, M. S. Briggs, & G. J. Fishman (New York: AIP), 345
- Colgate, S. A., & Leonard, P. J. T. 1993, in *AIP Conf. Proc. 307, Gamma-Ray Bursts*, ed. G. J. Fishman, J. J. Brainerd, & K. Hurley (New York: AIP), 21
- Coppi, P. S., Bulik, T., & Lamb, D. Q. 1996, in *AIP Conf. Proc. 384, Gamma-Ray Bursts*, ed. C. Kouveliotou, M. S. Briggs, & G. J. Fishman (New York: AIP), 358
- Cordes, J. M., Chernoff, D. F., & Wasserman, I. 1996, in *AIP Conf. Proc. 366, High-Velocity Neutron Stars and Gamma-Ray Bursts*, ed. R. E. Rothschild & R. E. Lingenfelter (New York: AIP), 11
- Duncan, R., & Li, H. 1997, *ApJ*, 484, 720
- Duncan, R., Li, H., & Thompson, C. 1993, in *AIP Conf. Proc. 280, Compton Gamma-Ray Observatory*, ed. M. Friedlander, N. Gehrels, & D. J. Macomb (New York: AIP), 1074
- Eichler, D., & Silk, J. 1992, *Science*, 257, 937
- Fenimore, E. E., et al. 1993, *Nature*, 366, 40
- Fenimore, E. E., Klebesadel, R. W., & Laros, J. G. 1996, *ApJ*, 460, 964
- Fishman, G. J. 1979, *ApJ*, 233, 851
- Fishman, G. J., Meegan, C. A., Watts, J. W., & Derrickson, J. H. 1978, *ApJ*, 223, 13
- Frail, D. A., Goss, W. M., & Whiteoak, J. B. Z. 1994, *ApJ*, 437, 781
- Frontera, F., et al. 1998, *ApJ*, 493, L67
- Fruchter, A., et al. 1997, *IAU Circ.*, 6747
- Graziani, C., Fenimore, E. E., Murakami, T., Yoshida, A., Lamb, D. Q., Wang, J. C. L., & Lored, T. J. 1992, in *Gamma-Ray Bursts: Observations, Analyses, and Theories*, ed. C. Ho, R. I. Epstein, & E. E. Fenimore (Cambridge: Cambridge Univ. Press), 407
- Graziani, C., & Lamb, D. Q. 1998, in *Proc. 4th Huntsville Symp., Gamma-Ray Bursts*, ed. C. Meegan & R. Preece (New York: AIP), in press
- Groot, P. J., et al. 1997, *IAU Circ.*, 6588
- Gurevich, A. V., Beskin, V. S., Zybin, K. P., & Ptitsyn, M. O. 1993, *JETP*, 103, 1873
- Hakkila, J., Meegan, C. A., Pendleton, G. N., Fishman, G. J., Wilson, R. B., Paciesas, W. S., Brock, M. N., & Horack, J. M. 1994, *ApJ*, 422, 659
- Hakkila, J., Meegan, C. A., Pendleton, G. N., Horack, J. M., Briggs, M. S., Paciesas, W. S., & Emslie, A. G. 1995, *ApJ*, 454, 134
- Harding, A. K. 1991, *Science*, 251, 1033
- Hartmann, D., Woosley, S. E., & Epstein, R. I. 1990, *ApJ*, 348, 625
- Hartmann, D. H., Greiner, J., & Briggs, M. S. 1995, *A&A*, 303, L65
- Higdon, J. C., & Lingenfelter, R. E. 1990, *AR&A*, 401
- in’t Zand, J. J. M., & Fenimore, E. 1994, in *AIP Conf. Proc. 307, Gamma-Ray Bursts*, ed. G. J. Fishman, J. J. Brainerd, & K. Hurley (New York: AIP), 692
- Jennings, M. C., & White, R. S. 1980, *ApJ*, 238, 110
- Kuijken, K., & Gilmore, G. 1989, *MNRAS*, 239, 571
- Lamb, D. Q. 1995, *PASP*, 107, 1152
- Lamb, D. Q., Bulik, T., & Coppi, P. S. 1996, in *AIP Conf. Proc. 366, High-Velocity Neutron Stars and Gamma-Ray Bursts*, ed. R. E. Rothschild & R. E. Lingenfelter (New York: AIP), 219
- Li, H., & Dermer, C. D. 1992, *Nature*, 359, 514

- Li, H., & Duncan, R. C. 1996a, in AIP Conf. Proc. 366, High-Velocity Neutron Stars and Gamma-Ray Bursts, ed. R. E. Rothschild & R. E. Lingenfelter (New York: AIP), 244
- . 1996b, in AIP Conf. Proc. 384, Gamma-Ray Bursts, ed. C. Kouveliotou, M. S. Briggs, & G. J. Fishman (New York: AIP), 366
- Li, H., Duncan, R., & Thompson, C. 1994, in AIP Conf. Proc. 307, Gamma-Ray Bursts, ed. G. J. Fishman, J. J. Brainerd, & K. Hurley (New York: AIP), 600
- Li, H., Fenimore, E. E., & Liang, E. P. 1996, ApJ, 461, L73
- Loredo, T. J., & Wasserman, I. 1996, ApJS, 96, 261
- . 1998a, ApJ, 502, 75
- . 1998b, ApJ, 502, 108
- Lyne, A. G., & Lorimer, D. R. 1994, Nature, 369, 127
- Meegan, C. A., Fishman, G. J., Wilson, R. B., Horack, J. M., Brock, M. N., Paciasas, W. S., Pendleton, G. N., & Kouveliotou, C. 1992, Nature, 355, 14
- Meegan, C. A., et al. 1996, ApJS, 106, 65
- Metzger, M. R., Kulkarni, S. R., Djorgovski, S. G., Gal, R., Steidel, C. C., & Frail, D. A. 1997a, IAU Circ., 6588
- Metzger, M. R., Cohen, J. G., Blakeslee, J. P., Kulkarni, S. S., Djorgovski, S. G., & Steidel, C. C. 1997b, IAU Circ., 6631
- Metzger, M. R., Cohen, J. G., Chaffee, F. H., & Blandford, R. D. 1997c, IAU Circ., 6676
- Miyamoto, M., & Nagai, R. 1975, PASJ, 27, 533
- Murakami, T., Fujii, M., Hayashida, K., Itoh, M., & Nishimura, J. 1988, Nature, 335, 234
- Narayan, R., & Ostriker, J. P. 1990, ApJ, 352, 222
- Paczynski, B. 1990, ApJ, 348, 485
- Podsiadlowski, P., Rees, M. J., & Ruderman, M. 1995, MNRAS, 273, 755
- Quashnock, J. M., & Lamb, D. Q. 1993, MNRAS, 265, L59
- Sahu, K., et al. 1997, Nature, 387, 476
- Schaefer, B. E. 1992, in Gamma-Ray Bursts: Observations, Analyses, and Theories, ed. C. Ho, R. I. Epstein, & E. E. Fenimore (Cambridge: Cambridge Univ. Press), 107
- . 1996, in AIP Conf. Proc. 384, Gamma-Ray Bursts, ed. C. Kouveliotou, M. S. Briggs, & G. J. Fishman (New York: AIP), 532
- Schaefer, B. E., et al. 1998, ApJ, submitted
- Shklovskii, I. S., & Mitrofanov, I. G. 1985, MNRAS, 212, 545
- Ulmer, A., Wijers, R. A. M. J., & Fenimore, E. E. 1995, ApJ, 440, L9
- Wasserman, I., & Salpeter, E. E. 1994, ApJ, 433, 670
- Woosley, S. E. 1993, in Proc. Conf., Caltech, Planets Around Pulsars, 355